Winter August 2014

Motion of Particles as a Probe: Dynamics and Assembly in Gel Networks/Aqueous Media

Cheol Hee Lee
University of Massachusetts - Amherst

MOTION OF PARTICLES AS A PROBE:

DYNAMICS AND ASSEMBLY IN GEL NETWORKS/AQUEOUS MEDIA

A Dissertation Presented

by

CHEOL HEE LEE

Submitted to the Graduate School of the

University of Massachusetts Amherst in partial fulfillment

of the requirements for the degree of

DOCTOR OF PHILOSOPHY

May 2014

Polymer Science & Engineering

MOTION OF PARTICLES AS A PROBE:

DYNAMICS AND ASSEMBLY IN GEL NETWORKS/AQUEOUS MEDIA

A Dissertation Presented

by

CHEOL HEE LEE

Approved as to style and content by:

_____

Alfred J. Crosby, Chair

_____

Ryan C. Hayward, Chair

_____

Todd Emrick, Chair

_____

Maria Kilfoil, Member

_____

David A. Hoagland, Department Head

Polymer Science and Engineering

DEDICATION

To my Dad (Dong Oh Lee), Mom (Ock Pai Kim), brother (Chanhee Lee), sister-in-law (Hoondeok Jung), and nephew (Jake Lee).

ACKNOWLEDGMENTS

It has been almost 6 years short and long at the same time.

Writing Acknowledgement seems like a confession.

First, I would like to thank all of my three advisors, Professor Alfred Crosby, Professor Todd Emrick, and Professor Ryan Hayward (alphabetical order!) who all have encouraged and supported me throughout this Ph.D. course. I sometimes think how difficult and challenging it would be to guide a student who belongs to three different groups. I really appreciate that all of you have tried to educate me to make me feel confident about what I have done in PSE department for the last 5 years. Of course, there have been moments when I almost gave up on this course, but talking with any of you always encouraged me to keep going forward even though you may not have noticed it. Al, I really appreciate that you eagerly tried to find me a research project that can fit into my thesis even though the subject is not quite with the group. Todd, I should thank you for saving me when I was looking for groups in my first year, and all the heartful encouragements you gave me from nowhere when it was really in need. Ryan, I have to say thank you for your biggest patience on me so that I could finish this project even after 5 years. Besides all of these aspects, I really enjoyed jokes Todd makes in group meetings that always crack me up even though it is sometimes very hard to catch what he means by them, Al's all-the-time gentleness as well as his nice sense of fashion, and Ryan's improvised physics equations and plots scribbled on a piece of paper, and your incredible intuition on science. I respect all of you as both mentors and scientists. My fourth committee member, Professor Maria Kilfoil, I feel very lucky that you are one of my committee members because you have given me so much valuable advices and discussions as

an expert in that research area. Thank you for your consistent willingness to help me with my research. I also like to thank Professor Jong-Man Kim, my advisor in Master's degree. I learned so much knowledge and skills on synthetic chemistry, and you fully encouraged and supported me so that I could go abroad for more study.

Approaching time to leave Amherst, I look back thinking that there could have been more things to remember with PSE friends. I would like to thank all of you from Crosby group, Emrick group, and Hayward group. I cannot even write down all the names here. Thanks to all of you, I enjoyed the variety of scientific areas all around me and easy access to answers whenever there were questions. I have nice and enjoyable memories with you all. I personally thank Ben and Sami that they both happily introduced me anything about what a life in US is like, which was very helpful to adapt myself to new place and lifestyle. I wish I had spent more times with you. I thank Spare Parts, Valley Radicals, and all classmates from 2008. Also, I thank the Korean society and friends from church in Amherst that helped me release stress away by sharing thoughts and burdens together. I guess you would know who they are without me listing names here. I would like to express my gratitude to PSE staff members to help PSE running smoothly and clean. Lisa and Vivien, thank you for everything you always do organize for students so that we can step by step approach the finish line.

My best friends in Korea, thank you all for being still friends with me even though I am not good at contacting you regularly. I did not have to bother myself explaining about how struggling I had been and what I had been doing here since you all are not interested at all. Awesome! I have saved the "PEN" for the last moment of this journey you guys got me as a gift in 2008. When I come back to Korea, we group together. Thanks guys!!

Finally, I must thank my family, who I owe so much love and many things that I cannot even think of paying back all. Dad (Dong Oh Lee) and Mom (Ock Pai Kim), thank you for your all-the-time prays and supports. You have raised and taught me as who I am now, which I am forever grateful for. My brother, Chanhee Lee, who came to US in the same year as me have been a best friend who I can rely on and talk to whenever it is needed. Sister-in-law, Hoondeok Jung, thanks for being by my brother supporting him throughout his graduate course, and also giving a birth to my precious nephew, Jake Lee. Love you all!

ABSTRACT

MOTION OF PARTICLES AS A PROBE:

DYNAMICS AND ASSEMBLY IN GEL NETWORKS/AQUEOUS MEDIA

MAY 2014

CHEOL HEE LEE, B.S., HANYANG UNIVERSITY

M.S., UNIVERSITY OF MASSACHUSETTS AMHERST

Ph.D., UNIVERSITY OF MASSACHUSETTS AMHESRT

Directed by: Professor Alfred J. Crosby

Professor Todd Emrick

Professor Ryan C. Hayward

Nanoparticles are of great interest with a wide variety of potential applications due to their unexpected but interesting physical properties which are different from bulk state, enable small length scale-driven transport through complex materials, and provide the building units for well-ordered structures. Observing the motion of nanoparticles provides information about surrounding microstructures, flow dynamics, and assembly processes by virtue of fluorescence of nanoparticles. However, the proper control of surface chemistry and the fluorescence of particles are both paramount and challenging to allow particles to be used in a quantitative and robust manner. This thesis describes the use of precisely-defined particles for characterizing and building complex structures. The research exploits advantages of the particle dynamics in three distinct studies: i) the tracking of single CdSe/ZnS core/shell QDs to characterize complex structures of hydrogels, ii) the transformation of dispersed QDs in

bulk phase into unique ring assemblies at the air/liquid interface, and iii) the mapping of flow dynamics within an evaporating droplet.

Chapter 2 describes the diffusion dynamics of single quantum dots (QDs) within polyacrylamide (PAAm) hydrogels to characterize the structural heterogeneity of gel networks by employing the single particle tracking (SPT) technique. Due to their photo-stable and highly fluorescent emission and its small size (4- 10 nm), individual QDs can be tracked by a fluorescence microscopy as they find pathways through structurally complex gel networks. This tracking provides information about spatiotemporal dynamics. The anomalous diffusion dynamics revealed by the motion of single QDs suggests that the structural heterogeneities of PAAm gels develop with increasing cross-linker content, and the length scales discovered are in a good agreement with the correlation length scale reported in the previous light scattering studies.

Chapter 3 describes the assembly of QD rings at the air/water interface by '2-D Pickering emulsions'. This work emanated from the unexpected observation of QD rings on the droplet of QD solutions. These rings form from QDs adsorbed to the interfacial line of surfactant islands assembled at the interface, and the QDs mark islands, appearing as rings. This island assembly was found to occur only at a specific range of surfactant concentrations due to the phase transition. Uniformly dispersed QDs in the bulk phase affording the ring patterns exclusively at the air/water interface provides insight that the thermodynamic driving force arises at the interfacial line between three phases (air/water/surfactant islands).

Finally, Chapter 4 details the radial flow dynamics within an evaporating droplet with a pinned contact line is investigated. By suspending and tracking fluorescent latex beads, the flow dynamics are quantified as a function of contact angle. This phenomenon, commonly

called the “coffee ring effect”, is advantageous for patterning and depositing suspended solutes on substrates. To develop evaporative assembly as a scalable process, it is particularly important to understand the effect of contact angle on radial velocity. By tracking the motion of suspended particles in a droplet, we experimentally measured the flow dynamics, specifically the height averaged radial velocity, within an evaporating droplet in the range of contact angles 5-50^{o}. We found that our experimental results are in a good agreement with the analytical prediction by Hu and Larson. Following the analytical predictions, we modified the original equation to a simplified equation that directly links radial velocity to contact angle and evaporation rate. This study provides insight into the manipulation of evaporative assembly processes on different substrates in terms of assembly kinetics and structural dimensions.

TABLE OF CONTENTS

Page

LIST OF TABLES

Table Page

LIST OF FIGURES

Figure Page

CHAPTER 1

INTRODUCTION

The observation of particle motions allows us to learn about the spatiotemporal information of the surrounding structures, e.g., microrheology [1], as well as particle dynamics [2] and underlying processes of material assembly. In this thesis, we study the motion of particles within different aqueous environments of interest where the locations of individual particles are detected by the fluorescent traces of probe particles, such as quantum dots (QDs) and dye-functionalized latex beads. To obtain useful information from particle motions, there are a few aspects to be considered. The determination of particle locations requires the different level of accuracy depending on the probe size and the spatiotemporal scale of interest. The surface chemistry rendering particles physically and photochemically stable in aqueous media is most important since probe particles in our study are subject to aqueous environments, and interactions between particle surface and surrounding structures should be avoided. This thesis consists of three works where fluorescent particles are utilized to obtain useful information from their motions. In the first work, the anomalous diffusion dynamics of single QDs, obtained by single particle tracking technique, are analyzed to obtain the information about the heterogeneous structure of surrounding gel networks which is known to inherently develop during random polymerization processes. Secondly, the formation of surfactant islands at the air/water interface is visualized by the adsorption of QDs to the interfacial line of surfactant islands, driven by a reduction of interfacial energy. Finally, the radial flow dynamics is explored by tracking individual latex beads within an evaporating droplet to find out the effect of contact angle on the radial flow velocity.

1.1 The Anomalous Diffusion Dynamics of Single Quantum Dots within Heterogeneous PAAm Hydrogels

Hydrogels are chemically or physically crosslinked hydrophilic polymer networks immersed in water. They show interesting physical properties, such as elasticity, swelling property, toughness, permeability, turbidity, and mass transport property,[3-8] which make hydrogels applicable to many applications, e.g., water absorbent, shock absorber, artificial tissue scaffold, and drug delivery.[9-11] These properties, however, are readily affected by the extent of structural heterogeneity of hydrogels, which is known to inherently develop during the radical polymerization process as a function of crosslinker content.[12] For example, the elastic modulus of polyacrylamide hydrogels increases with crosslinker content up to ~ 3 mol% relative to monomer after which the modulus begin to decrease.[13] This transition point of the elastic modulus is due to the structural heterogeneity taking effect on bulk properties at ~ 3 mol% crosslink content.[13] Briefly, the structural heterogeneity of hydrogels is attributed to the fluctuation of local polymer density developed by the non-ideal crosslinking processes, e.g., backbiting crosslinks (cyclization), and due to hydrophobicity and higher reactivity of crosslinkers. Single particle tracking (SPT) is a useful technique for the characterization of complex structures since understanding the motion of nanoparticle can provide time-scale and length-scale-dependent information about the properties of structurally complex matrix materials. The SPT technique allows us to investigate the dynamics of single QDs as well as obtain information about the heterogeneous structures of crosslinked polymer networks without destroying and/or perturbing the materials structures by analyzing the trajectories of single QDs moving within polymer hydrogels.

The continuous time random walk (CTRW) has been a popular formalism to successfully describe the stochastic transport or dynamics within diverse complex media, as first proposed by Montroll and Weiss.[14] For example, the CTRW has been applied to explain anomalous dynamics within a cell and on the membrane as well as stochastic dynamics in finance and share prices in stock markets.[15] In the CTRW, a random walker spends a certain time at random by being localized or trapped before making a step showing a random distribution of caging times which is an indicator of the extent of structural heterogeneities.

In this work, we are determined to utilize SPT technique to investigate and characterize the nature of structural heterogeneity of PAAm hydrogels by analyzing the distribution of caging times obtained from experimental diffusion dynamics of single QDs.

1.2 The Assembly of Quantum Dot Rings by 2-D Pickering Emulsions

Patterning and assembling nanoparticles (NPs) have been of interest in a broad range of scientific areas, such as photonic, electronic and magnetic devices for sensing and optics.[16] Using NPs as a building block, nano- and microscale ordered structures are constructed on substrates by many assembly methods, e.g., template-based process, which are both time-consuming and costly.[16-18]

This work presents a simple method of assembling QDs into rings at the air/water interface, which was unexpectedly observed from an evaporating droplet. It was noticed that the formation of QD rings occurs only on specific substrates, the cover glass with a trace amount of unknown impurities on its surface. A trace amount of impurity, playing a critical role, leaches into a bulk phase of water containing PEGylated QDs and reaches the air/water

interface most likely due to the surface active property. Once the amount of impurities at the interface is in the right concentration range, they form round islands due to its coexistence of gas (G) and liquid expanded (LE) phases.[19, 20] These islands play a role of templates for QDs adsorbing into the interfacial line of islands, a process driven by a reduction in interfacial energy. We successfully reproduced this phenomenon, the formation of QD rings, on cleaned glass with the addition of surfactants to prove our hypothesis. In addition, the deposition and patterning of QD rings on large area substrate is demonstrated employing a dip-coating method.

1.3 Flow Dynamics within Evaporating Droplets

Deegan's first paper explaining about the 'coffee ring effect' in 1997 is one of the most cited papers thus far.[21] Due to the inherently non-uniform evaporation flux along the droplet interface with contact angles < 90^{o}, there is a radial flow generated from the center towards the edge to compensate more loss of water at the edge. The 'coffee ring effect' has been an underlying phenomenon in many mass transport-driven assemblies of solutes, such as microshperes, DNA, polymers, and nanoparticles, in evaporating droplets.[22-27] There have been many theoretical works studying the radial flow velocity as function of evaporation time, contact angle, surfactant concentration, the size of droplets, etc,[28-30] as opposed to experimental study. Here we present the empirical observation of the flow dynamics, by tracking individual latex beads as a probe, within an evaporating droplet to verify analytical predictions. Particularly, the effect of contact angle on the radial flow velocity is examined since we are interested in the impact of contact angle on the kinetics and/or the dimensions of the ordered structures constructed by the flexible blade flow coating technique. [31]

We found that our experimental observation of the effect of contact angle on the radial flow velocity agrees well with analytical predictions by Hu and Larson, and modified their analytical equation to a simple equation which directly links radial flow dynamics to contact angle and evaporation rate, thus providing an intuitive understanding of the influence of contact angle.

1.4 Thesis Overview

In the following chapters, works will be delivered in detail to address how the motion of particles is utilized in each study. In Chapter 2, anomalous diffusion dynamics of single QDs within polyacrylamide (PAAm) hydrogels will be described by tracking single QDs, providing useful information about the structural heterogeneities which is affected by the content of cross-linkers. This result will provide an insight to the heterogeneous, but interconnected elastic structures of hydrogels. In Chapter 3, patterning and assembly of QD rings will be demonstrated, which was originated from unexpected observations leading to finding of an interesting assembly phenomenon. QD rings are assembled by being adsorbed to the interfacial line of surfactant islands which are assembled at the air/water interface. The transfer and patterning of these QD rings onto different substrate will be demonstrated using dip coating technique. In Chapter 4, we will quantify the radial flow dynamics as a function of contact angle in evaporating droplets by tracking suspended fluorescent latex particles. This is, to our knowledge, the first empirical demonstration of radial flows as a function of contact angle whose results are consistent with the analytical predictions by Hu and Larson. Furthermore, we will modify the original prediction to a simpler form such that it directly relates the radial flows to contact angles as well as evaporation rates. Collectively, these

works and results presented here allow us to utilize the spatiotemporal information obtained from the motion of particles to explain and/or describe surrounding structures as well as assembly processes.

1.5 References

1. Mason, T.G., et al., *Particle Tracking Microrheology of Complex Fluids.* Physical Review Letters, 1997. **79**(17): p. 3282.

2. Kim, M., S.M. Anthony, and S. Granick, *Activated Surface Diffusion in a Simple Colloid System.* Physical Review Letters, 2009. **102**(17): p. 178303.

3. Bansil, R. and M.K. Gupta, *Effect of Varying Crosslinking Density on Polyacrylamide Gels.* Ferroelectrics, 1980. ***30***(1-4): p. 63-71.

4. Fawcett, J.S. and C.J.O.R. Morris, *Molecular-sieve chromatography of proteins on granulated polyacrylamide gels.* Separation science, 1966. ***1***: p. 9-26.

5. Richards, E.G. and C.J. Temple, *Some Properties of Polyacrylamdie Gels.* Nature Physical Science, 1971. ***230***: p. 92-96.

6. Valentine, M.T., et al., *Investigating the microenvironments of inhomogeneous soft materials with multiple particle tracking.* Physical Review E, 2001. **64**(6): p. 061506.

7. Weiss, N. and A. Silberberg, *Inhomogeneity of polyacrylamide gel structure from permeability and viscoelasticity.* British Polymer Journal, 1977. ***9***(2): p. 144-150.

8. Zhang, J., C.R. Daubert, and E.A. Foegeding, *Characterization of polyacrylamide gels as an elastic model for food gels.* Rheologica Acta, 2005. ***44***(6): p. 622-630.

9. Hoare, T.R. and D.S. Kohane, *Hydrogels in drug delivery: Progress and challenges.* Polymer, 2008. ***49***(8): p. 1993-2007.

10. Drury, J.L. and D.J. Mooney, *Hydrogels for tissue engineering: scaffold design variables and applications.* Biomaterials, 2003. ***24***(24): p. 4337-4351.

11. Lutolf, M.P., *Biomaterials: Spotlight on hydrogels.* Nat Mater, 2009. ***8***(6): p. 451-453.

12. Bastide, J. and L. Leibler, *Large-scale heterogeneities in randomly cross-linked networks.* Macromolecules, 1988. ***21***(8): p. 2647-2649.

13. Calvet, D., J.Y. Wong, and S. Giasson, *Rheological Monitoring of Polyacrylamide Gelation: Importance of Cross-Link Density and Temperature.* Macromolecules, 2004. **37**(20): p. 7762-7771.

14. Montroll, E.W. and G.H. Weiss, *Random Walks on Lattices .2.* Journal of Mathematical Physics, 1965. **6**(2): p. 167.

15. Scalas, E., *The application of continuous-time random walks in finance and economics.* Physica A: Statistical Mechanics and its Applications, 2006. **362**(2): p. 225-239.

16. Chen, J., et al., *Evaporation-Induced Assembly of Quantum Dots into Nanorings.* ACS Nano, 2008. **3**(1): p. 173-180.

17. Babayan, Y., et al., *Templated and Hierarchical Assembly of CdSe/ZnS Quantum Dots.* Advanced Materials, 2004. **16**(15): p. 1341-1345.

18. Gleiche, M., L.F. Chi, and H. Fuchs, *Nanoscopic channel lattices with controlled anisotropic wetting.* Nature, 2000. **403**(6766): p. 173-175.

19. Henon, S. and J. Meunier, *Microscope at the Brewster angle: Direct observation of first-order phase transitions in monolayers.* Review of Scientific Instruments, 1991. **62**(4): p. 936-939.

20. Kaganer, V.M., H. Möhwald, and P. Dutta, *Structure and phase transitions in Langmuir monolayers.* Reviews of Modern Physics, 1999. **71**(3): p. 779-819.

21. Deegan, R.D., et al., *Capillary flow as the cause of ring stains from dried liquid drops.* Nature, 1997. **389**(6653): p. 827-829.

22. Deegan, R.D., *Pattern formation in drying drops.* Physical Review E, 2000. **61**(1): p. 475-485.

23. Jing, J., et al., *Automated high resolution optical mapping using arrayed, fluid-fixed DNA molecules.* Proceedings of the National Academy of Sciences, 1998. **95**(14): p. 8046-8051.

24. Kim, H.S., et al., *Nanoparticle Stripes, Grids, and Ribbons Produced by Flow Coating.* Advanced Materials, 2010. **22**(41): p. 4600-4604.

25. Senses, E., et al., *Spatial Ordering of Colloids in a Drying Aqueous Polymer Droplet.* Langmuir, 2013. **29**(8): p. 2588-2594.

26. Truskett, V.N. and K.J. Stebe, *Influence of Surfactants on an Evaporating Drop: Fluorescence Images and Particle Deposition Patterns.* Langmuir, 2003. **19**(20): p. 8271-8279.

27. Yunker, P.J., et al., *Suppression of the coffee-ring effect by shape-dependent capillary interactions.* Nature, 2011. **476**(7360): p. 308-311.

28. Hu, H. and R.G. Larson, *Evaporation of a Sessile Droplet on a Substrate.* The Journal of Physical Chemistry B, 2002. **106**(6): p. 1334-1344.

29. Hu, H. and R.G. Larson, *Analysis of the Effects of Marangoni Stresses on the Microflow in an Evaporating Sessile Droplet.* Langmuir, 2005. **21**(9): p. 3972-3980.

30. Hu, H. and R.G. Larson, *Analysis of the Microfluid Flow in an Evaporating Sessile Droplet.* Langmuir, 2005. **21**(9): p. 3963-3971.

31. Lee, D.Y., et al., *Macroscopic Nanoparticle Ribbons and Fabrics.* Advanced Materials, 2013. **25**(9): p. 1248-1253.

CHAPTER 2

CHARACTERIZATION OF HETEROGENEOUS POLYACRYLAMIDE HYDROGELS BY TRACKING OF SINGLE QUANTUM DOTS[1]

2.1 Introduction

Polymer gels, consisting of either chemically or physically cross-linked networks of polymer chains immersed in solvent, possess interesting and useful physical properties.[1] In particular, hydrogels are attractive materials for use as tissue scaffolds[2, 3] and as media for drug delivery[4] and separations,[5] due to their high water content, potential for biocompatibility, and highly tunable stiffness and permeability. However, the physical characteristics of gels, including their elasticity, permeability, turbidity, swelling propensity, mass transport properties, and fracture toughness are known to be sensitive to the presence of structural heterogeneities in the network [6-11] that in most cases arise inherently due to the random nature of the cross-linking process.[12] Thus, the ability to characterize, understand, and ultimately control structural heterogeneity of gel networks is important to tailoring their properties.

Polyacrylamide (PAAm) gels are among the most commonly applied and well-studied hydrogel material systems due to their utility for high resolution electrophoretic separation of proteins and DNA,[13] and more recently as cell culture substrates that provide

[1] Reprinted and adapted with permission from *Macromolecules* 2014, *47* (2), pp 741-749, DOI**:** 10.1021/ma402373s. Copyright © 2014 American Chemical Society.

physiologically relevant stiffness.[14, 15] The structure of PAAm hydrogels have previously been examined using scattering techniques (light, X-ray, and neutron),[16-18] transmission electron microscopy (TEM),[19, 20] chromatographic methods,[9] and electrophoresis.[21] For example, Geissler and coworkers used a combination of scattering techniques to show that PAAm hydrogels containing 8 wt% acrylamide monomer, with various contents of *N*,*N*'-methylene bisacrylamide crosslinker, contain significant structural heterogeneities with sizes ranging from 2.5 Å to several hundred nm.[16] Small angle X-ray and neutron scattering measurements showed excess forward scattering at small q, indicating the presence of frozen heterogeneities in structure.[16, 17] Similarly, dynamic light scattering measurements yielded position-dependent speckle patterns characteristic of spatial heterogeneities, which at high crosslink density cause the gels to become opaque and increasingly fragile.[22] Fawcett and Morris conducted chromatography experiments using PAAm gel beads containing 6 - 15 wt% acrylamide, and found that the elution volume of protein solutions first decreased with increasing concentration of cross-linker, but then subsequently increased.[9] Both sets of studies suggest that increased cross-linker content leads to formation of high-density bundles of polymer chains that are tightly crosslinked due to local enrichment of the relatively hydrophobic cross-linkers, interconnected by lower density regions with a characteristic pore size that actually grows larger with increasing cross-linker content.[9]

Despite this work, our understanding of structural heterogeneity within even this important and well-studied class of materials remains largely incomplete, reflecting the fundamental challenges inherent to characterization of irregular nano-scale structures in solvated systems. From scattering and chromatographic measurements, one obtains only characteristic structural length scales that reflect spatial averages over large volumes of

material. Electron microscopy, while enabling high spatial resolution, suffers from difficult and invasive sample preparation and the possibility for significant imaging artifacts, and is generally poorly suited to capture dynamics within the material.

Fluorescence-based single particle tracking (SPT) methods provide powerful tools to investigate dynamics within complex media with high spatial resolution, since the position of each moving object can be located with a precision well below the optical diffraction limit by identifying the centroid of fluorescence intensity.[23, 24] Such methods have been employed to study dynamics in a diverse range of heterogeneous systems, including lipid membranes [24, 25] and the cytoplasm,[26, 27] particles in block copolymer membranes,[28] analyte molecules in mesoporous sensors,[29, 30] reactions on catalyst surfaces,[31] networks undergoing gelation,[32] and nanopost arrays.[33] The motion of individual fluorescent molecules within PAAm gels[34] and surface bound poly(*N*-isopropylacrylamide) brushes[35] has been followed using SPT, in both cases revealing confined and heterogeneous motion of the probe molecules. These experiments, however, use individual dye molecules whose largest dimensions are only 1-2 nm, thus they are presumably only sensitive to the very smallest pores in these polymer structures, and may actually be adsorbing onto the polymer network due to hydrophobic interactions.

On the other extreme in terms of probe size, the Weitz[8, 36] and Granick[37] groups have investigated the dynamics of fluorescent sub-micrometer colloidal particles within networks of the semi-flexible biopolymer F-actin. In these cases, non-diffusive motion was observed, corresponding to probe particles making infrequent jumps between pores in which their motion is highly restricted.[36, 37] Similar processes of rare, activated hops between confined microenvironments are ubiquitous for a wide range of material systems approaching

gelation or glass transitions, with the characteristic feature that the distribution of displacements deviates from Gaussian statistics by showing a long exponential tail at large displacements.[38-41]

A variety of models have been used to describe heterogeneous dynamics within complex/disordered media.[42-44] One of the most commonly employed approaches is the continuous time random walk (CTRW) formalism first introduced by Montroll and Weiss,[45] in which a random walker waits for a certain time at any given site before making a jump to a neighboring site. A simple choice for the distribution of these 'caging times' comes from the random trap (RT) model, where each site on regular lattices is characterized by a trapping energy selected at random from a distribution that describes the heterogeneity of the complex medium. A caged particle at each site advances to neighboring sites by thermally-activated hopping mechanism with a jumping frequency dependent on the trapping energy. The RT model has been successfully employed to describe aspects of glassy phenomenology,[40, 46, 47] electronic transport in disordered solids,[48, 49] desorption dynamics in porous activated carbon grains,[50] and protein dynamics.[51]

In this chapter, we demonstrate that SPT of individual quantum dots (QDs) provides a simple and useful method to characterize structural heterogeneity within PAAm hydrogels. While tracking of single QDs has commonly been employed to understand transport processes within cells,[52-55] this method has not yet been widely applied in synthetic materials. We choose core/shell CdSe/ZnS QDs as probe particles, since they have high photoluminescence and photostability, allowing for straightforward tracking of single particles by standard epifluorescence microscopy over long periods of time. In addition, the hydrodynamic diameter of the QDs used here is around 20 nm, which represents an intermediate size

between the small molecule dyes (~ 1 – 2 nm) and colloidal particles (~ 100 nm - 1 μm) more commonly used for SPT studies, and which more closely match the characteristic structural sizes of synthetic hydrogels such as PAAm. We find that QDs show sub-diffusive behavior and non-Gaussian displacement distributions, consistent with prior reports on motion through heterogeneous media. We also analyze the distribution of caging times in the context of a simple random trap (RT) model for the energy landscape within the gel, and find that the characteristic trap energy increases for larger crosslink densities, consistent with greater heterogeneity of these networks.

2.2 Experimental

2.2.1 Reagents

Tri-*n*-octylphophine oxide (technical grade), cadmium acetate dihydrate, hexamethyldisilathiane, anhydrous methanol, 11-mercaptoundecanoic acid (95%), and tetramethylammonium hydroxide (25% in methanol) were purchased from Sigma-Aldrich. Tri-*n*-octylphosphine (97%) was from Strem Chemicals. Selenium (200 mesh 99.999%) and diethylzinc (15 wt% in hexane) were from Alfa Aesar. All reagents were used without further purification.

2.2.2 Synthesis of CdSe/ZnS Core/Shell Quantum Dots

TOPO (tri-*n*-octylphosphine oxide) capped CdSe/ZnS core/shell QDs were synthesized following a modified version of the previously described procedure.[56, 57] To a 3-neck, 25 mL round-bottom flask equipped with reflux condenser, N_2 inlet, septum, and

thermocouple probe were added cadmium acetate (0.375 mmol) and tri-*n*-octylphosphine oxide (TOPO, 7.5 g). The mixture was heated to 150 ^{o}C under vacuum for 15 min. The temperature was then increased to 300 ^{o}C, after which a solution of selenium (5.1 mmol) in tri-*n*-octylphosphine (TOP, 2 mL) was swiftly injected. The nanocrystals were allowed to grow at 280 ^{o}C for 4 min where the color of the solution gradually changed from yellow to red. Then, the temperature was reduced to 160 ^{o}C for shell growth. A precursor solution containing Zn and S was prepared by dissolving diethylzinc (15 w% in hexane, 0.45 mmol) and hexamethyldisilathiane (0.45 mmol) into tri-*n*-octylphosphine (3 mL) inside a glove box and then administered into the reaction pot using syringe pumps at a rate of 1 mL/hr. The solution was allowed to cool to room temperature, and the TOPO-covered CdSe nanoparticles were isolated by precipitation into methanol with a few mL of chloroform. The solution was centrifuged and the supernatant decanted. The resulting solid was purified by dissolution in chloroform, precipitation into methanol, and centrifugation. The red powder isolated from this process was dried under a purge of N_2 and stored in chloroform or toluene.

2.2.3 Water Soluble CdSe/ZnS Core/Shell Quantum Dots

The CdSe cores are determined to be ~ 4 nm in diameter from UV/Vis absorption spectra,[58] while the ZnS shell size is ~ 1 nm confirmed by TEM. A ligand exchange was conducted to replace TOPO with 11-mercaptoundecanoic acid, rendering the QDs dispersible in water. For ligand exchange, a QD solution containing 2 mg of QDs was added to a 4 mL glass vial and dried under N_2 to form a thin layer of QDs. Next, 0.3 - 0.4 mL of anhydrous methanol, 11-mercaptoundecanoic acid (MUA, at least a 10-fold excess by weight relative to QDs), and tetramethylammonium hydroxide (25 wt% in methanol, 2 eq. to MUA) were

placed in the vial under N_2. The mixture was stirred overnight at 60 ^{o}C and precipitated by adding 1 mL of hexane with a small amount of chloroform. The solution was centrifuged and the supernatant decanted. The red powder was dissolved in deionized water and purified to remove residual ligand through a centrifuge tube filter with 100 kg/mol molecular weight cutoff.

An important consideration in SPT measurements is the possibility for adsorption of QDs to the polymer network, which may influence particle motion. However, a previous micro-rheological study of crosslinked PAAm sols and gels revealed that latex beads with carboxylate and amidine surface functionalities show identical behavior, suggesting that particle interactions with polymer networks is not critical for these specific functionalities.[59] Thus, the carboxylate ligands used here presumably yield minimal adsorption of QDs to the network. By contrast, QDs with poly(ethylene oxide) (PEO, MW = 600 Da) ligands, prepared according to a literature procedure,[60] were found to show substantially slower motion compared to those with carboxylate ligands, likely due to hydrogen bonding interactions between PAAm and PEO.

2.2.4 Optical Properties of MUA Capped CdSe/ZnS Core/Shell Quantum Dots

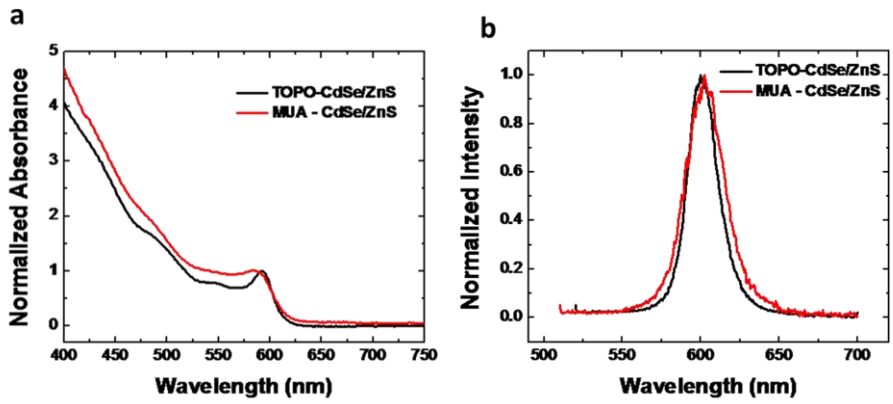

Figure 0.1. (a) UV-Vis spectra of CdSe/ZnS QD solution before and after ligand exchange from TOPO to MUA ligand. (b) Photo luminescence spectra before and after ligand exchange.

2.2.5 Synthesis of DHLA-PEG600

DHLA-PEG600 ligand was synthesized by following literature methods. [61, 62] Thioctic acid (5.0 g, 24 mmol), poly(ethylene glycol) (MW = 600, 145 g, 242 mmol), a catalytic amount of 4-(dimethylamino)-pyridine (890 mg, 7.3 mmol), and CH_2Cl_2 (240 mL) were combined in a flask and degassed with N_2. The mixture was cooled to 0 ^oC in an ice bath, and a solution of dicyclohexylcarbodiimide (6.5 g, 31 mmol) in CH_2Cl_2 (20 mL) was added dropwise. The mixture was stirred overnight at room temperature. The precipitate was filtered over a plug of Celite, and the residue was mixed with an aqueous sodium bicarbonate solution, and extracted with ethyl acetate (3 times). The combined organic phase was dried over $MgSO_4$, filtered, and evaporated to give a yellow oil. This oil was purified by column chromatography on silica gel (chloroform/methanol 95:5), and the product recovered as a yellow oil (~ 60 %). Sodium borohydride (13.8 mmol) in a 1:4 ethanol/water (55 mL) was used to reduce the disulfide, giving PEG-DHLA.

2.2.6 Fabrication of PAAm Hydrogels and Quantum Dot Loading

PAAm hydrogel samples were prepared by the conventional free radical polymerization in aqueous solutions containing 7 wt% acrylamide monomer, and either 0.3, 0.7, 1.1, or 1.5 mol% *N,N*'-methylenebisacrylamide cross-linker (expressed relative to monomer plus crosslinker). The pre-gel solution containing acrylamide and bisacrylamide were degassed to remove oxygen, then tetramethylethylenediamine and ammonium persulfate (10% solution) added in respective amounts of 1 μL and 5 μL per 1 mL of pre-gel solution, and the mixture was immediately transferred into a 1 mm gap between glass slides. Following 30 - 60 min for gelation, the slides were separated and PAAm gels were allowed to swell to equilibrium in water for at least 48 h to extract unreacted monomer, initiator, and accelerator. Compared to the as-prepared state, gels increased in linear dimension upon swelling by 7-30% for 1.5 - 0.3 mol% crosslinker concentrations.

QDs were loaded into PAAm hydrogels by immersing half of a piece of gel (~ 10 x 20 mm lateral dimensions) into an aqueous solution containing 0.2 - 0.5 nM QDs, while the other half was exposed to air. The resulting flux of water into the gel, driven by evaporation from the portion in contact with air, led to convective loading of QDs into the gel. This method allows for transport of QDs to distances of ~ 20 - 30 μm within the gel over a time of ~ 36 h, which is much more rapid than for passive transport of particles into fully submerged gels. This procedure naturally generates a gradient in QD number density as a function of position from the gel surface; all measurements reported here were conducted with the focal plane located ~ 20 μm below the free surface, as this yielded a sufficient density of QDs for tracking and should be sufficiently far into the gel to minimize any surface effects. Additionally, this procedure serves to prevent large aggregates from entering the gel. We do

not directly incorporate QDs into the pre-gel solution due to quenching of fluorescence by the free radical initiator.

2.2.7 Single Quantum Dot Tracking

The motion of QDs was imaged by video epifluorescence microscopy (Zeiss Axiovert 200) using a 100×, oil-immersion objective (Zeiss) with a numerical aperture of 1.4 and a Retiga 2000R CCD camera (Q-Imaging), such that each pixel corresponded to a region of 72 × 72 nm in the sample. A region of interest of 400×400 pixels was studied, and these imaging conditions yield a point-spread function (PSF) with a standard deviation of 110 nm. In each frame, the positions of the QDs were identified using a publicly available particle tracking algorithm based on the work of Grier and Crocker [63] and adapted to MATLAB by Blair and Dufresne,[64] which finds the brightness averaged centroid position with sub-pixel accuracy. This sub-pixel positioning accuracy of individual particles allows for the video based particle tracking to be a powerful technique over the diffraction limited resolution of microscopy imaging that is given by a following equation, $R = 0.6\frac{\lambda_{em}}{N.A.}$. R is the diffraction limited resolution, λ_{em} is the emitting light wavelength, and N.A. is the numerical aperture of the objective used, where R is approximately a few hundred nanometers. Since a single QD is 5 nm in diameter much smaller than R, it is critical to accurately pinpoint the location of individual particles. In Figure 2.2, the tracking accuracy was determined by observing stationary QDs bound to a glass slide, which yielded a standard deviation in the mean position of ~ 20 nm (~ 0.3 pixel). We note that the possibility to image single QDs (at 10 – 20 frames per second) using a cooled CCD camera without intensification relied on two key factors: the high brightness of these core/shell QDs, and the use of a custom filter set providing

broadband excitation (320 – 450 nm), which takes advantage of the greatly increased absorption coefficient of CdSe QDs for high energy excitation.[58] Blinking of the immobilized QDs confirmed that single QDs, rather than aggregates, could be localized at 10 - 20 frames per second. Additional experiments conducted using an electron-multiplied CCD (Andor iXon Duo 897) and an ORCA-flash 4.0 scientific CMOS camera (Hamamatsu) yielded similar results to those conducted with the cooled CCD, although with better signal-to-noise ratios even at higher frame rates (50 fps).

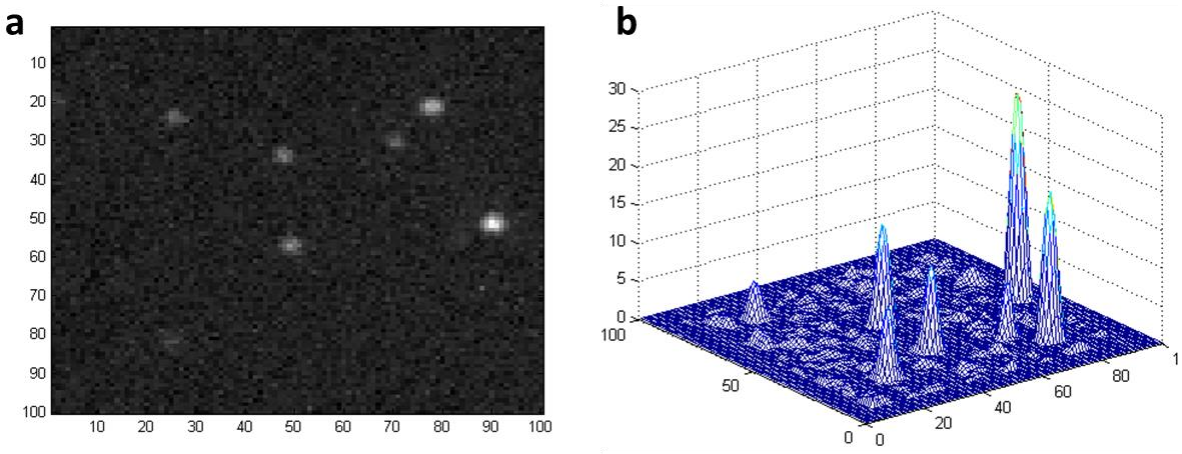

Figure 0.2. (a) Fluorescence microscope image of single QDs immobilized on glass slide. (b) 3-D intensity profile of single QDs corresponding to QDs from (a) after image processing.

2.3 Parameters of the MATLAB Particle Tracking Algorithm

In order to execute the MATLAB particle tracking algorithm, a few parameters need to be determined, such as ‘maxdisp’, ‘memory’, and the threshold for the particle intensity. ‘maxdisp’ refers to the maximum displacement that individual particles are expected to move during a certain time interval. ‘maxdisp’ should be set to a value somewhat less than the mean spacing between particles. Since in our experiments the number density of particles was

adjusted to have a large enough spacing between particles, ‘maxdisp’ was set to 10 pixels (720 nm) every 50 ms based on the diffusion coefficient (~20 $\mu m^2/s$) of particles with 10 nm hydrodynamic radius in pure water. A particle is unlikely to jump so far in this time scale.

The ‘memory’ parameter is the number of time steps that a particle can be 'lost' and then recovered again. If the particle reappears after this number of frames has elapsed, it will be tracked as a new particle. This is useful if particles occasionally disappear from the field of view, especially practical for the tracking of single QDs because of their blinking. ‘memory’ parameter was set to a value based on the blinking statistics; how many number of frames it takes to come back to “on” state once QDs enter “off” state (dark state). In Figure 2.3a is shown QD blinking statistics, the distribution of off times, which is described by a power law $P(\tau_{off}) \sim \tau_{off}^{-1.5}$, τ_{off} is the time duration of dark state, consistent with previous reports.[65] Figure 2.3b presents the cumulative probability of “off” times suggesting that approximately 99% of QDs become “on” state within 0.5 sec. Therefore, ‘memory’ was set to 10 for 20 fps videos and 5 for 10 fps videos. We found qualitatively consistent QD dynamics from a lower number density of QDs in the field of view with two parameters set as determined above, which makes reliable analyses in terms of particle misrecognition.

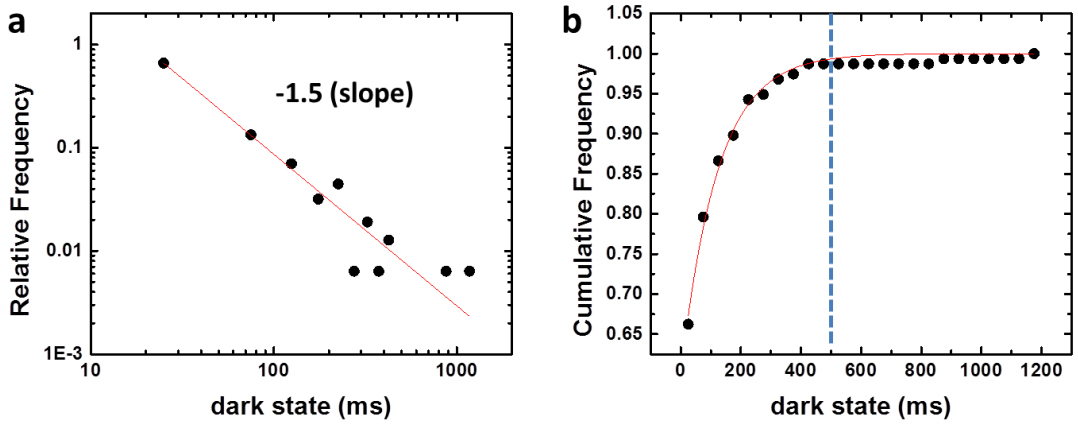

Figure 0.3. (a) probability distribution of off times of QDs (b) cumulative probability distribution of off times of QDs.

The threshold for the particle intensity from the background noise is critical for the consistent image processing. Before determining the threshold, each image is convolved with two kernels, Gaussian and boxcar. The original image is first treated with Gaussian kernel to smooth things out and then treated with boxcar kernel to remove any features (particles) above the background noise. By subtracting the boxcar version from the Gaussian version, images are flattened with residual noise which is above the mean noise. The distribution of residual noise is described by a Gaussian with a zero center with a variance of noise in Figure 2.4a. We chose the threshold noise at 4 times standard deviation of the Gaussian fit so that there is only 0.006% chance of misrecognizing a noise as a particle, which is corresponding to ~10 pixels out of 160000 pixels in the region of interest (400×400 ROI). In Figure 2.4b is shown the application of threshold noise (4σ) to the experimental intensity profile, showing that peaks above the threshold (dotted red line) are recognized as particles.

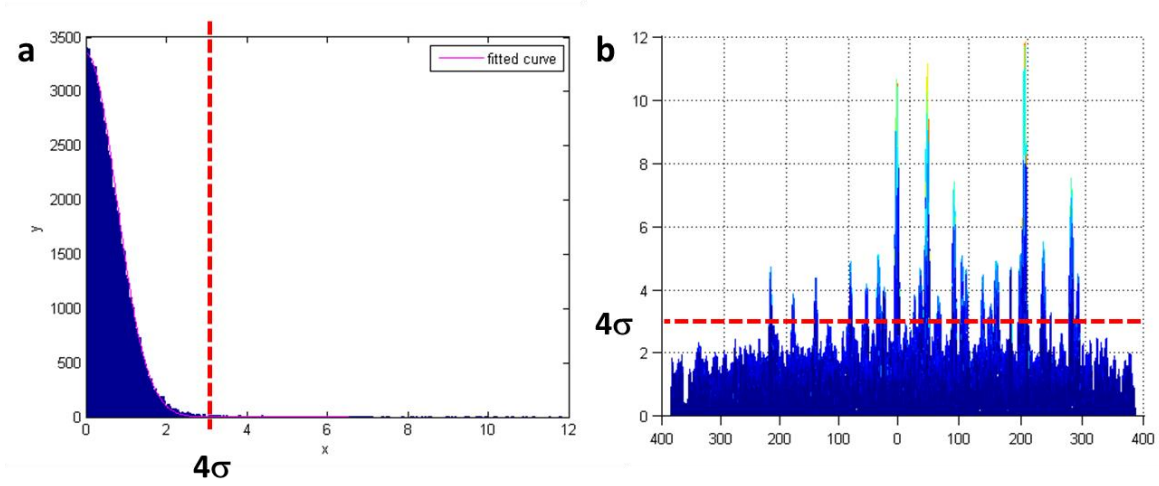

Figure 0.4. (a) Noise threshold is indicated as a dotted red line at 4 times standard deviation (σ) of a Gaussian fit. (b) Application of threshold determined from (a) to the experimental intensity profile indicating reasonable separation between residual noises and particles.

2.4 Continuous Time Random Walk (CTRW)

The Continuous time random walk (CTRW) is the stochastic/disorder model first introduced by Montoll and Weiss. [45] For example, the CTRW has been applied to successfully explain anomalous dynamics within a cell and on the plasma membrane as well as stochastic dynamics in finance and share prices in stock markets.[66] In the CTRW, the number of jumps n made by the walker in a time interval Δt is a random variable. That is, a random walker does not make a jump on a regular basis in the CTRW. A random walker makes a jump after waiting for a time $t1$ and waits for another time period $t2$ before making the next jump. It is not expectable how long time period it would wait before making a jump. The time period between subsequent jumps is called 'caging time' or 'waiting time'. Furthermore, each jump length by a random walker is also a random variable. If these two

variables, i.e. caging times and jump lengths, are statistically independent, it is called a decoupled CTRW.

2.4.1 Models of Disordered Systems

A random walker experiencing CTRW is considered on regular lattices with different transition rates. This is a common approach for modeling diffusion in complex media. This modeling captures the concept of random waiting time distribution due to different transition rates, but it does not do so for random jump length distribution because a random walker makes jumps of a discrete length on regular lattices. Here are some common disorder models introduced.

Random Barriers (RB)

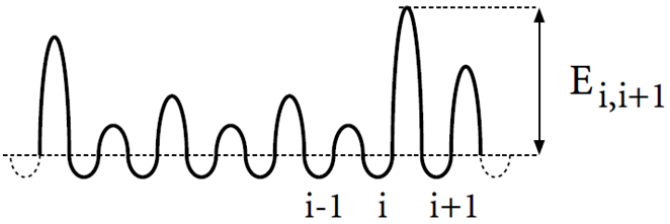

In this model the transition rates between neighboring sites have the symmetry which are given by an Arrhenius law,

$$J_{i,i+1} = J_{i+1,i}$$

$$J_{i,i+1} = J_0 \exp\left(\frac{-E_{i,i+1}}{k_B T}\right) \qquad E_{i,i+1} \geq 0$$

where $J_{i,\,i+1}$ is the transition rate from the i to the site i+1 when i and i+1 are neighboring sites, and $E_{i,\,i+1}$ is the barrier energy that restricts the transition of particles and is distributed over the lattices by a probability density function (PDF) $P_B(E)$.

Random Trap (RT)

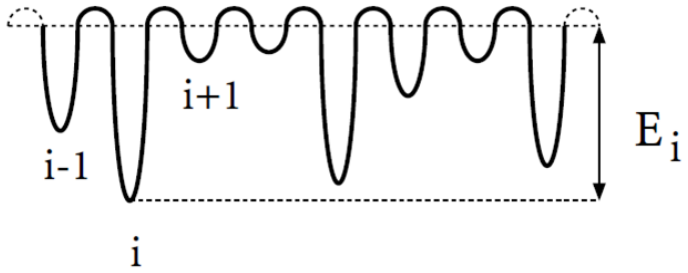

In this model, the transition rates from one site to all neighboring sites are equal, which are given by an Arrhenius law,

$$J_i = J_0 \exp\left(\frac{-E_i}{k_B T}\right) \qquad E_i \geq 0$$

where J_i is the transition rate at the site i to any neighboring sites, and E_i is the trap energy at the site i which is taken by a PDF $P_T(E)$.

Combination of RB and RT

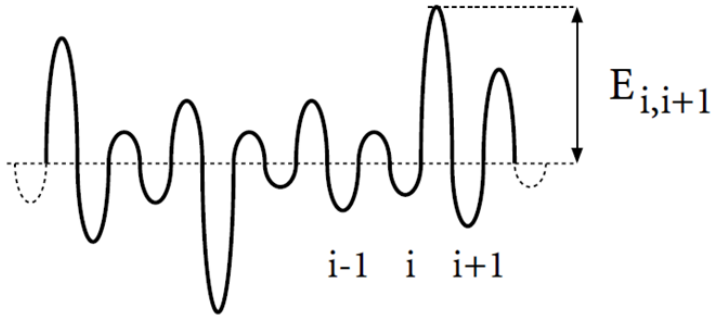

$$J_{i,i+1} = J_0 \exp\left(\frac{-(E_{i,i+1} + E_i)}{k_B T}\right) \qquad E \geq 0$$

The transition rates of the combined RB and RT model are given as shown above. $E_{i,\,i+1}$ and E_i are taken independently from the distribution $P_B(E)$ and $P_T(E)$.

2.5 Results and Discussion

2.5.1 Mean Square Displacement

The motion of individual QDs within polyacrylamide gel matrices is determined from time series of epifluorescence images taken with a frame rate of 10-20 fps using tracking algorithms described previously.[63, 64] Blinking of each particle is observed, both for QDs within the gel and for those immobilized on glass slides, providing confirmation that the particles being tracked are individual QDs, rather than aggregates. Furthermore, analysis of the diffusive motion of QDs in water/glycerol mixtures (10:90 wt%) reveals a hydrodynamic radius of 10.7 ± 2.2 nm, using a literature value for the viscosity of water/glycerol mixtures,[67] in good agreement with the value of ~ 10 nm determined by dynamic light scattering for particles dispersed in water (in Figure 2.5). This hydrodynamic radius is ~ 2 times larger than the estimated geometric radius of ~ 4.5 nm based on known core and shell sizes and the estimated thickness of the ligand shell, consistent with previous reports showing similar increases in hydrodynamic size due to trapping of a large solvation layer around each QD by the hydrophilic carboxylate ligands.[68]

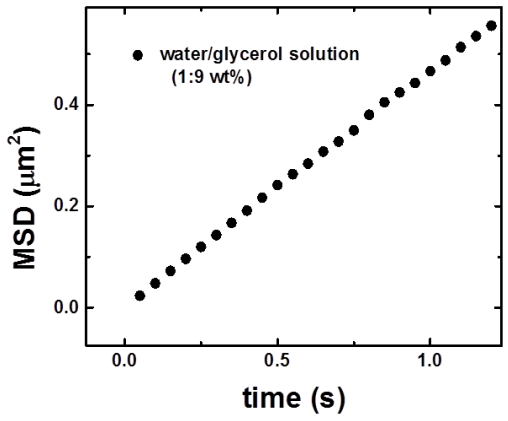

Sample #	D from MSD (um^2/s)	R_h (S-E eq.) (nm)
1	0.09	10.6
2	0.12	7.9
3	0.08	11.9
4	0.07	13.6
5	0.1	9.5
Avg.	**0.09 ± 0.02**	**11 ± 2**

Figure 0.5. (left) An example of MSD plot of single QDs diffusing in a 90 wt% glycerol aqueous solution shows a linear relationship between MSD and time, indicating Brownian motion of single QDs. (right) Table summarizing results of five single QD particle tracking experiments in a glycerol aqueous solution confirms that the hydrodynamic size of a single QD calculated by Stokes-Einstein equation matches the size obtained from dynamic light scattering experiments.

We prepare PAAm gel samples containing a fixed initial monomer concentration of 7 wt% and crosslinker contents of 0.3, 0.7, 1.1, or 1.5 mol%, with all gels swelled to equilibrium before loading of QDs. These compositions were chosen as they provide sufficiently large porosities to admit convective loading of QDs across a wide range of crosslinker content. Representative trajectories for single QDs moving within the extreme cases of 0.3 and 1.5 mol% crosslinker are shown in Figure 2.6a and b, respectively. Clear qualitative differences are seen, with the trajectories in the low crosslink density sample (Figure 2.6a) appearing almost diffusive, while those in the high crosslink density sample (Figure 2.6b) reveal many QDs that remain trapped within a small region of the gel

throughout the full duration of the particle tracking experiment (120 s). Within each gel, there is also significant variability in the extent of motion for different particles, and most particles show intermittent confinement, changing in time between low- and high- mobility states which is well shown in Figure 2.7. All of these observations are consistent with the presence of a distribution of different microenvironments within the network, as is common for complex media including polymer networks, colloidal suspensions, and glassy systems.[39, 47]

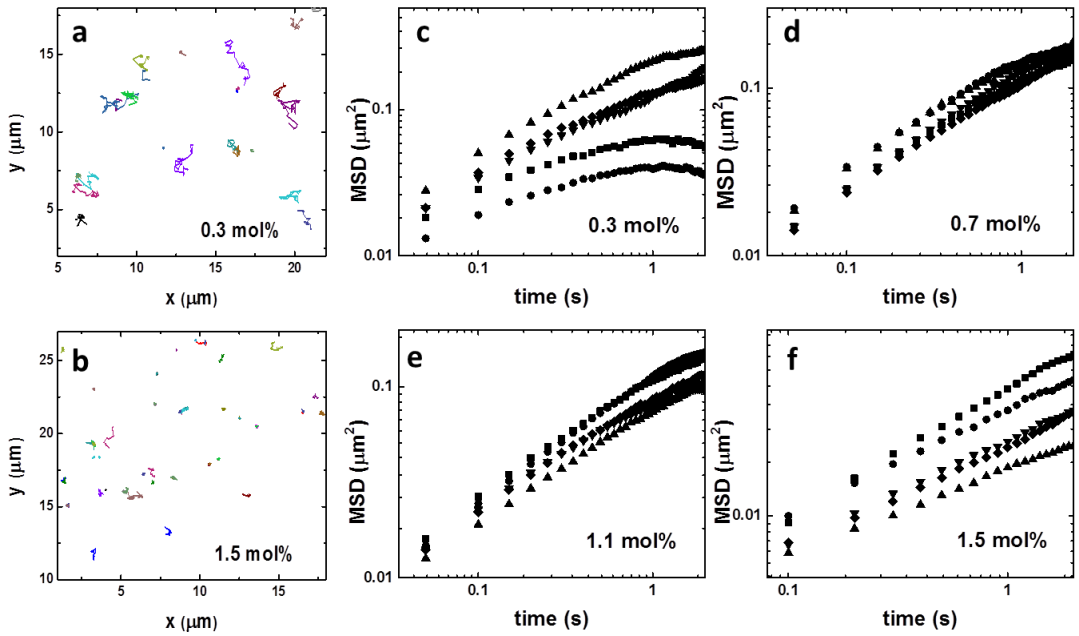

Figure 0.6. (a,b): Representative trajectories of single QDs moving within 7 wt% PAAm hydrogels containing (a) 0.3 mol% and (b) 1.5 mol% crosslinker within a 17 x 17 μm region of interest. Each plotted trajectory is between 2 and 3 s in duration. While heterogeneity is evident in both cases, QDs show much greater mobility in the more lightly crosslinked sample. (c-f): Ensemble averaged MSD plots at five randomly selected locations within gels of different crosslinker content, revealing subdiffusive behavior with considerable variability

even within each sample. The different symbols correspond to five different randomly chosen locations within a gel of each gel composition.

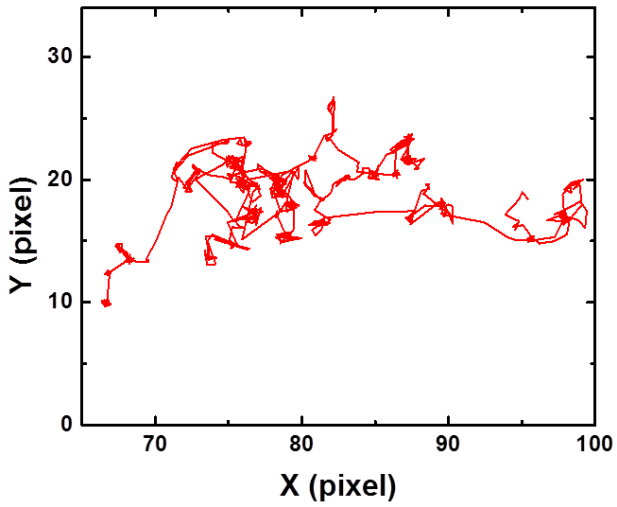

Figure 0.7. Representative trajectory of a QD suggesting intermittent confinements, changing in time between low- and high- mobility states.

It is difficult to completely exclude the possibility that adsorption of QDs to the polymer network plays a role in the observed motional heterogeneities, however we do not expect strong interactions between the particles—coated with carboxylate ligands that are substantially ionized at neutral pH—and the PAAm network. By contrast, QDs functionalized with poly(ethylene glycol) (PEG) ligands (MW = 600 Da) show substantially reduced mobilities compared to those with carboxylate ligands, most likely due to hydrogen bonding interactions between PAAm and PEG. Table 2.1 summarizes the sub-diffusion exponent values for both PEG- and MUA-QDs within a gel at the same composition suggesting that PEG-QDs show reduced mobilities (smaller exponent value) compared to MUA-QDs.

Additionally, the amide groups in PAAm can undergo hydrolysis to yield some degree of anionic character to the network; this would inhibit absorption to the network, but also raises the possibility that electrostatic interactions between the particle and gel may play a role. However, based on a previous study showing little change in gel structure after 5 days of storage in water for similar gel compositions,[69] we expect the effects of hydrolysis to be minimal. In addition, a previous micro-rheological study of latex beads within crosslinked PAAm sols and gels found identical behavior for particles with negative (carboxylate) and positive (amidine) surface functionalities, suggesting that particle interactions with the network are relatively unimportant.[59] Regardless of the exact nature of the interactions of the QDs with the PAAm network, however, their motion clearly reveals the presence of heterogeneity in the gel structure.

Table 0.1. MSD sub-diffusion exponent values for MUA (carboxylate)-QDs and PEG-QDs within a gel of 7wt% 0.3mol% composition. PEG-QDs show a lower value of MSD exponent suggesting PEG-QDs are more restricted in motion in PAAm gel networks.

MSD subdiffusion exponent value		
	7wt% 0.3mol%	
sample#	MUA	PEG600
1	0.72	0.52
2	0.68	0.38
3	0.73	0.57
Avg.	**0.71 ± 0.03**	**0.5 ± 0.1**

To quantify the motion of QDs, we first consider the most commonly used metric for characterization of sub-diffusive behavior in single particle tracking experiments, i.e., the

ensemble-averaged mean-square displacement (MSD) $\left\langle \Delta r^2 \right\rangle = \left\langle \left| r(t+\tau) - r(t) \right|^2 \right\rangle$ as a function of lag time τ. The angular brackets indicate an average over all starting times *t*, and all particle trajectories collected for a given region of the gel (typically several thousand trajectories). In Figure 2.6(c-f) we show MSD plots for five different spatial positions chosen randomly for each of the four gel compositions (represented by the different symbols). All twenty curves exhibit sub-diffusive behavior, i.e., MSD ~ τ^{γ}, with $0 < \gamma < 1$, indicating that the gel network restricts particle movement in all cases. In Table 2.2, we summarize values of γ for each gel composition averaged across the five different locations, with uncertainties representing standard deviations. The values are all in the range of 0.5 – 0.7, and with the exception of the 0.3 mol% sample, the data suggest a slight trend of decreasing γ with increasing crosslinker content.

Further examination of the data for the 0.3 mol% sample shows that for the regions of the gel that yield the two smallest values of γ (circle and square markers in Figure 2.6c), the measured MSD actually *decreases* after a lag time of roughly 1 s, by an amount larger than the uncertainties estimated from the standard error of the mean. This decrease in MSD with time is a clearly unphysical result that apparently arises because the rapidly moving particles diffuse out of the focal plane or the field of view within a relatively short time, while the highly confined particles can be tracked for much longer time. Thus, with increasing lag time, the MSD value is increasingly dominated by the contribution of a relatively small number of nearly immobile particles. In other words, at least for long lag times, the calculated MSD does not represent a true ensemble average, but instead reflects sampling biased in favor of the slowly moving particles. It remains unclear whether the variability in density of slow particles—and correspondingly in the MSD plots—from position to position within the

sample (separated by a few mm) reflects real changes in structure, i.e., a greater density of trapping sites in some regions, or simply limited sampling statistics. Nonetheless, these results highlight the inherent difficulty of interpreting MSD curves for motion in heterogeneous media, a result appreciated in prior studies.[35, 70]

Table 0.2. Best fit values of γ, β, and A^2 from different gel compositions

Crosslinker (mol%)	0.3	0.7	1.1	1.5
γ *	0.6 ± 0.1	0.72 ± 0.03	0.65 ± 0.03	0.5 ± 0.1
β **	0.33 ± 0.01	0.38 ± 0.01	0.34 ± 0.01	0.31 ± 0.01
A^2 ($\mu m^2/s^{2\beta}$) **	0.144 ± 0.008	0.090 ± 0.006	0.058 ± 0.001	0.023 ± 0.001

* uncertainties represent one standard deviation

** uncertainties represent standard error of best fits

2.5.2 Van Hove Function (Displacement Distribution of a Single Particle)

We next consider the van Hove correlation function $G(\Delta x, \tau)$, which describes the probability for a single particle to undergo a displacement by a distance of Δx from its starting position along a given dimension after a lag time τ (in practice, displacements along both the *x*- and *y*-directions are analyzed). This method has previously been shown to provide more robust characterization of the dynamics of particles in disordered media [8, 37-40] since unlike MSD analysis, it allows for a separation of the dynamics of slow and fast moving particles. Example of van Hove functions for several values of τ are shown in Figure 2.8a for

a gel containing 0.7 mol% cross-linker. The data for short displacements can be well-described by a Gaussian (as shown in the inset to Figure 2.8a); however, the breadth of this Gaussian does not broaden in time as for diffusive motion, but instead remains nearly constant, indicating that it corresponds to the local motion of trapped particles. At larger displacements, the van Hove functions show broad non-Gaussian tails that can be well described by an exponential dependence, $G(\Delta x, \tau) \sim \exp(\frac{-|\Delta x|}{\lambda(\tau)})$, where $\lambda(\tau)$ is the characteristic length scale of displacements within the exponential tail regimes $P(\Delta x, \tau) \sim \exp(\frac{-\Delta x}{\lambda})$.

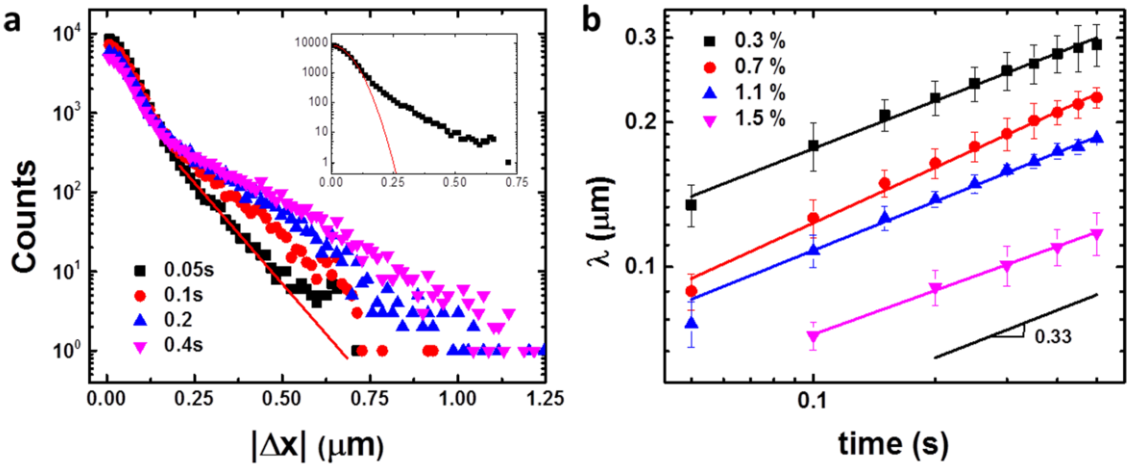

Figure 0.8. (a) The van Hove functions for several lag times in a 7 wt% PAAm gel containing 0.7 mol% crosslinker show exponential tails that evolve in time. The red solid line is the exponential fit for a lag time of 0.05 s. The inset shows a Gaussian fit (red solid line) to the short displacement data for a 0.05 sec lag time. (b) The characteristic decay length of the exponential tail, $\lambda(\tau)$, is plotted against lag time, revealing power-law dependences with exponents close to 0.33 (best fit values β are summarized in Table 2.2).

This form of the van Hove function—Gaussian for short displacements with an exponential tail—has been reported in a diversity of contexts including colloidal particles in a variety of complex fluids [8, 36, 37] and systems close to glass or jamming transitions [38-41], and is apparently a rather generic feature of subdiffusive motion in heterogeneous systems. The broad exponential tail stems from relatively rare events corresponding to large displacements between local microenvironments. In the case of jammed or glassy materials, these events represent the escape of a particle from the cage formed by its neighbors.[38] For F-actin gels, they represent the jumping of a particle out of a local trap that has a mesh size comparable to the particle dimensions.[8, 36]

In the current PAAm gel system, we interpret the rare events as illustrated in Figure 2.9a, namely as QDs escaping from one cage and into a neighboring cage. We find the characteristic displacement where the distribution crosses over from a Gaussian to an exponential dependence to be $|\Delta x| \sim 100–140$ nm for all four gel compositions. We interpret this value as the characteristic size of trapping sites ξ_T, within which the QDs are able to undergo essentially diffusive motion (importantly, this ability of even caged particles to undergo sizable displacements provides further evidence that restricted motion does not reflect adsorption of QDs to the PAAm network). Notably, ξ_T is much larger than the characteristic mesh sizes of ~ 3 – 5 nm determined previously by scattering,[16, 17] indicating that the cages are not defined by the primary mesh, but instead arise from larger-scale structural features in the gel. The presence of structural features on these length scales is consistent with previous scattering studies on gels of similar composition,[16] as well as reports that PAAm gels begin to lose their optical clarity at slightly higher crosslinker concentrations of ~ 2-3 mol%.[11, 69] We suggest that the trapping sites correspond to

cavities or channels that have a lower density of polymer and/or crosslinks, surrounded by a denser polymer mesh. It is known from prior studies that during the early stages of PAAm gel formation, denser polymer regions (or 'microgels') rich in crosslinker form, due to the higher reactivity and hydrophobicity of bisacrylamide compared to acrylamide.[71] We speculate that as these microgels percolate to yield a macroscopic gel, and are filled in by additional polymerization, they define an interconnected set of dense regions that are largely inaccessible to the QD probes due to their small mesh size. The surrounding regions, which are more lightly-crosslinked and possibly lower in polymer content, provide largely interconnected pathways for QD motion, but with dead-ends and local constrictions that yield trapping sites. Motion of a QD from one such trap to another is therefore presumably limited by a free energy barrier *E* associated with the probability of a QD entering into a small constriction between neighboring traps.

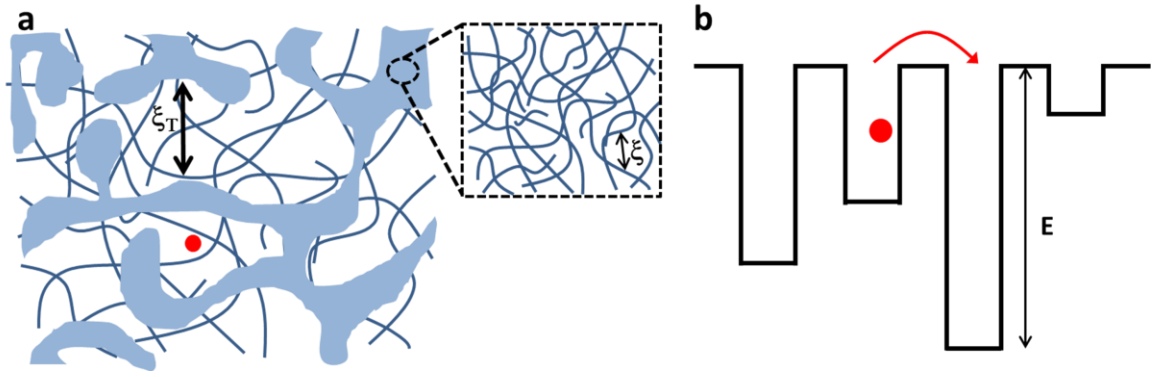

Figure 0.9. (a) An illustration of the proposed heterogeneous microstructure of PAAm gels, and trapping of QDs in cages of size ξ_T due to an energy barrier associated with the probability of a QD entering into a small constriction between neighboring traps formed by percolated microgels with primary mesh size ξ. (b) Schematic of a 1-D random trap (RT) model. Each lattice site has a different trap energy depth, $E > 0$, selected from a given

distribution. The frequency of escape events from each site is assumed to follow an Arrhenius dependence with activation energy E.

2.5.3 Macroscopic Sub-diffusive Coefficient

The characteristic length scale of the exponential tail, $\lambda(\tau)$, grows with lag time, as plotted in Figure 2.8b for each of the four different gel compositions. These data represent averages over all five spatial regions analyzed for each composition, with error bars representing standard deviations. Unlike the MSD plots, the van Hove functions reveal consistent behavior between different regions of the sample. For a given value of τ, there is clear variability between the different gel compositions, with λ monotonically decreasing as crosslinker content is increased. Since λ is dependent upon how often probe particles make rare jumps, this finding suggests that higher cross-linker concentrations provide more restrictive traps, and/or a higher density of trapping sites. For each composition, a power-law dependence $\lambda(\tau) = A\tau^{\beta}$ is found to accurately describe the data, with the best fit values of A^2 and β summarized in Table 2.2. Wang et al., reported the dependence $\lambda(\tau) \sim \tau^{0.5}$ for several different material systems exhibiting anomalous diffusion, suggesting a rather universal origin of this behavior.[37] Here, we find slightly lower values of $\beta \approx 0.33$, suggesting that the PAAm gels do not follow quite the same behavior. However, while the estimated uncertainties on the best-fit exponents are narrow enough to distinguish them from 0.5, we caution that our data cover only one decade in τ. Since $\lambda(\tau)$ represents the characteristic length over which an ensemble of particles will move through the network in a time τ, from the relationship $\lambda^2(\tau) = A^2\tau^{2\beta}$, we identify A^2 as analogous to a macroscopic (sub-)diffusion

coefficient. As seen in Table 2.2, while β is nearly constant as a function of crosslinker, A^2 decreases by approximately an order of magnitude from the gels containing 0.3 mol% crosslinker to those containing 1.5 mol%.

2.5.5 Random Trap Model & Caging Time Distribution

To further characterize the structural heterogeneity of PAAm gels, we turn to the distribution of QD caging times, as motivated by the continuous time random walk (CTRW) formalism,[45] which is commonly applied to understand anomalous diffusion dynamics.[38-40] Within this framework, the motion of a random walker is characterized using two parameters: the distribution of caging times between successive jumps, and the jump length taken in a given step. As a simple model for the structure of heterogeneous PAAm gel networks, we consider the random trap (RT) model, where particles undergo jumps of fixed size between sites, as shown schematically in Figure 2.9b, with the trapping energy at each site E randomly selected from a given distribution $P(E)$.[47] The escape of particles from a trap with depth E is assumed to follow an activated (Arrhenius) dependence, thus yielding an escape rate

$$J = J_o \exp(\frac{-E}{k_B T}) \ , \tag{1}$$

where J_o is the jump attempt frequency and $k_B T$ is thermal energy.

While clearly an oversimplification in several respects, we suggest that this model provides a reasonable starting point to describe the stochastic motion of QDs between different micro-environments in the PAAm hydrogel networks. In the simplest case of an exponential distribution of trapping energies [47, 72]

$$P(E) = \frac{1}{E_c} \exp(\frac{-E}{E_c}) \quad , \tag{2}$$

where $E \geq 0$, and E_c represents the average energy trap depth, the model yields a distribution of caging times [47, 72, 73]

$$\rho(t_c) = \frac{\alpha}{J_o^{\alpha}} t_c^{-(\alpha+1)}, \tag{3}$$

with $\alpha = \frac{k_B T}{E_c}$ describing the magnitude of the characteristic trapping energy relative to the amount of thermal energy available for particles to escape.

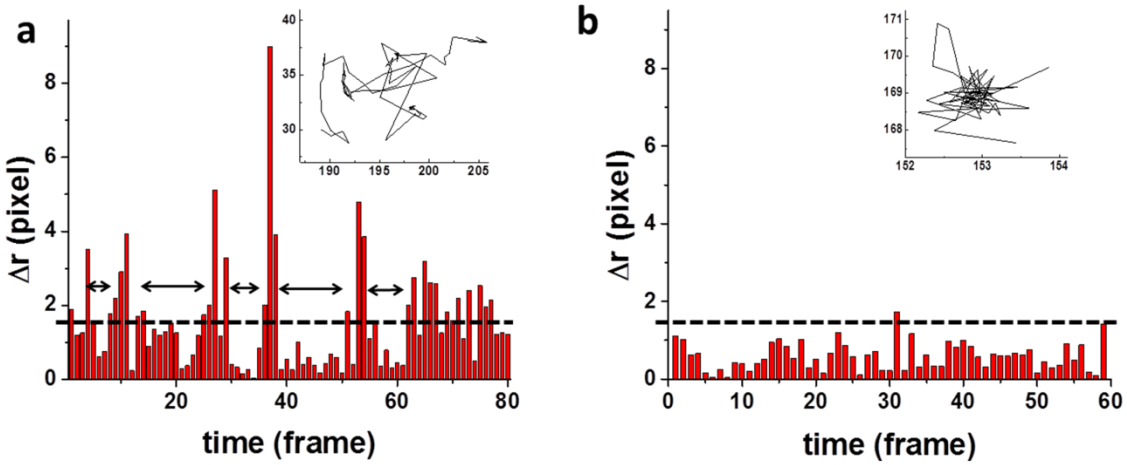

Figure 0.10. The two-dimensional displacement in pixels between successive time points in particle trajectories is plotted to illustrate the classification of caging events: (a) A representative trajectory for a particle undergoing relatively free motion and (b) a highly caged particle. The dotted line represents the jump threshold selected, while the arrows represent caged portions of the trajectory identified in this manner (only some caging events are indicated). Insets are trajectories for each particle (axes in pixels).

To compare with the predictions of the RT model, we extract the distribution of caging times from individual QD trajectories, following the method of Gao, et al.[38] The two-dimensional displacement Δr between succesive frames is plotted as a function of time, and jumping events are identified by displacements larger than a certain threshold, as indicated by the dotted lines in Figure 2.10. As examples, Figure 2.10a shows a particle that undergoes many jumps during the period of observation, while Figure 2.10b shows the motion of a confined QD that undergoes only one jump above the threshold. The time duration between successive jumps is thus identified as the length of a single caging event, and a histogram of the frequency of caging times is constructucted from all particle trajectories. In this procedure, it is critical to choose an appropriate jump threshold. For example, Figure 2.11 shows caging time distributions constructed for gels with 1.5% cross-linker for different jump thresholds. For the initial portion of the curve (up to caging times of ~ 1 s) the data are well-described by a power law $\rho(t_c) \sim t_c^{-(\alpha+1)}$, in accordance with the predictions of the RT model with exponentially distributed barriers, as in equation (3). However, the value of the exponent α decreases substantially with increases in the jump threshold, in this case from -2 to -1.2 with changes in threshold from 0.5 to 2.0 pixels. Notably, the initial slopes for the largest jump thresholds (1.7 and 2.0 pixels) are similar values, which is consistent with the values of α reaching a plateau for sufficiently large thresholds, as we discuss further below. For longer caging times, the behavior seems to transition to a steeper power law that is less sensitive to the choice of threshold, but due to the relatively poor statistics in this region, we cannot confidently say whether this represents a qualitative change in behavior, as opposed to, e.g., limited sampling of the high energy traps.

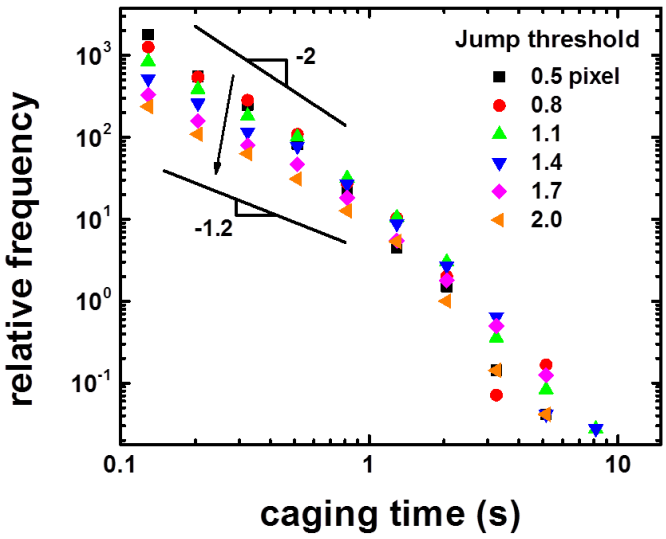

Figure 0.11. The evolution of caging time distribution for 1.5 mol% gel composition as a function of jump threshold in pixel. The slope gradually decreases from - 2 to -1.2 as the jump threshold is changed from 0.5 to 2.0 pixels (36 – 144 nm).

One route to choose an unambiguous jump threshold is by considering the ensemble-averaged van Hove function (Figure 2.8), where the crossover from Gaussian to exponential statistics at ξ_T provides a natural choice to describe the transition from caged to uncaged motion. Here, we do so by extracting the point where the Gaussian and exponential fits to the van Hove functions cross, yielding values of α for each gel composition as summarized in Table 2.3 and plotted in Figure 2.12 for 0.3 and 1.5 mol% gels. In Figure 2.12, the fitted solid lines by power law work well for short caging times whereas a slight deviation is shown for long caging times. This can be explained by three reasons: i) the analytical equation does not predict well for long caging times, ii) the experimental time scale (2 minutes) is not long enough to catch those particles dwelling in cages for longer times, and iii) QDs are excluded from very small cages in the first place. Experimental caging time distribution following the

prediction of RT model indicates that our system is close to equilibrium state at least for short caging times, which satisfies Boltzmann statistics used for the jumping frequency of a particle, equation (1).

We also extract values of α for a range of different jump thresholds, and plot the results for each gel composition, as in Figure 2.13. Remarkably, each plot shows an initial sensitivity to jump threshold at small values, but then reaches a plateau value beyond a threshold ranging from about 1.1 pixels for 0.3 mol% crosslinker to 1.5 pixels for 1.5 mol% crosslinker. The values of α determined from the plateau regions in Figure 2.13 are in a very good agreement with α values obtained by using crossover points as jump thresholds, providing further confidence that this procedure yields a robust characterization of the caging time distributions. Further, the jump threshold at which the value of α reaches this plateau value can also be interpreted as a characteristic size-scale associated with the traps. In this case, we obtain estimates of $\xi_T \sim 80 - 110$ nm, slightly smaller than the values of $\sim 100 - 140$ nm obtained from the crossover point of the van Hove functions, though still in reasonable agreement.

Table 0.3. Average values of α and E_c determined from the crossover points for each gel composition.

	0.3 %	0.7 %	1.1 %	1.5 %
Crossover point (nm)	130 ± 10	134 ± 2	135 ± 8	100 ± 10
α *	1.02 ± 0.27	0.6 ± 0.1	0.52 ± 0.09	0.3 ± 0.1
E_c (k_BT)	1 ± 0.3	1.7 ± 0.3	1.9 ± 0.3	3.3 ± 1.1

* uncertainties represent one standard deviation

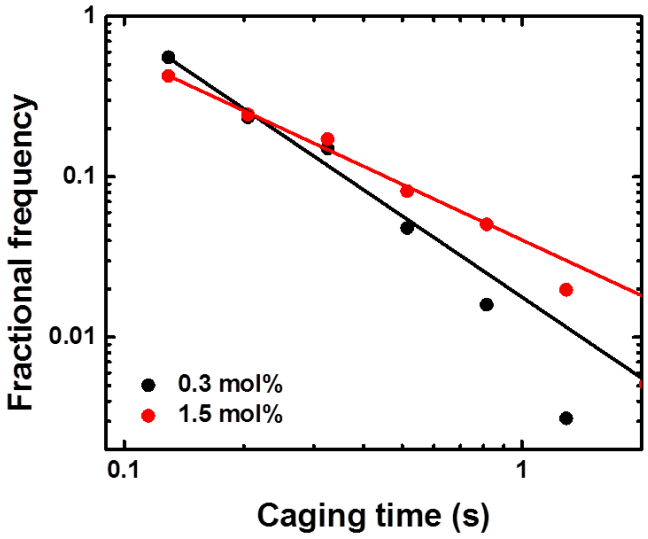

Figure 0.12. Experimental caging time distribution for 0.3 and 1.5 mol% cross-linker density gels. The solid lines are power law fits showing a good description of experimental data for caging times up to 1 sec, whereas a slight deviation for longer caging times. High crosslink density gel sample shows a broader distribution of caging times than low crosslink density one.

Although the values of α at 0.7 and 1.1 mol% are the same to within uncertainty, the overall trend of decreasing α with increasing crosslink density is clear. Interpreted in terms of the RT model with an exponential distribution of trap energies, these data indicate average trap depths of 1 k_BT in the most lightly crosslinked sample, 1.7 – 1.9 k_BT for intermediate crosslinker concentrations, and 3.3 k_BT for the most densely crosslinked sample. Presumably, the larger trap energies for the more highly crosslinked gels reflect the presence of a greater steric barrier for the QD probes to pass through the constrictions separating neighboring cages. These results are qualitatively consistent with the overall slower motion and greater frequency of highly trapped particles for the more highly crosslinked samples. They also imply that the more highly crosslinked gels are more heterogeneous, in the sense that a larger average trap depth E_c also implies a broader distribution of trap energies. Finally, we note that these results are largely consistent with prior studies on structural heterogeneity in PAAm gels at low to modest crosslinker concentration, in particular the findings of Fawcett and Morris that the permeability of PAAm gels to proteins decreases with increasing crosslink content up to ~ 3 mol%.[9]

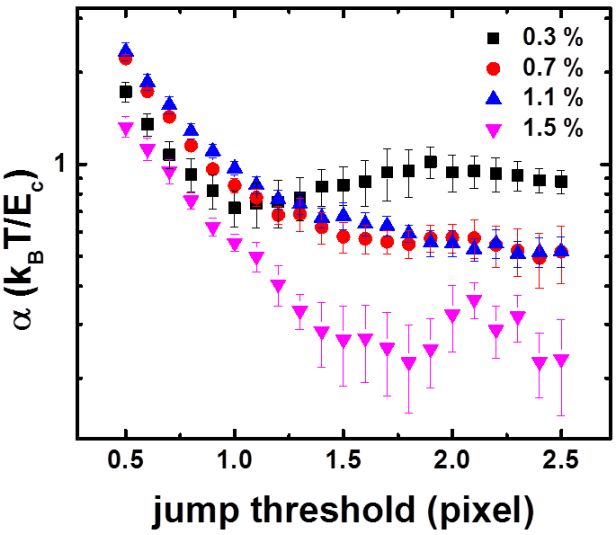

Figure 0.13. Values of α extracted from the initial slope of the caging time distributions are plotted as a function of the jump threshold for each gel composition studied. The values initially decrease for small thresholds, but then reach a plateau above a threshold of ~1.5 pixel.

2.5.6 Local Dynamics of Free & Confined Quantum Dots

We studied the local dynamics of free and confined QDs to examine polymer density in and outside traps. For experiments, an ORCA-flash 4.0 scientific CMOS camera (Hamamatsu) was used to record images at higher speed, 50 fps. Free and confined particles are separated using jump thresholds determined above and MSD plots are constructed for five different spatial positions for 0.7-1.5 mol% gels. In Figure 2.14 are shown MSD plots for both free and confined particles of 1.5 mol% gel sample. To estimate the diffusion coefficient for each group, we used the first one and first five data points with zero intercept for free and confined particles, respectively. Using diffusion coefficient determined from MSD plots, local

viscosities are also estimated using Stokes-Einstein equation which are all summarized in Table 2.4. Despite the limited number of data points for free particles (because they get trapped again soon), MSD plots show diffusive motions, while MSDs for confined particles evidently plateau within 0.1 second. As shown in Table 2.4, the diffusion coefficient for free particles is generally ~6 times larger than confined ones, thereby larger viscosities were estimated for confined regions with a slightly increasing trend with increasing crosslink content. We are, however, not confident about these findings because many data points could be missing in MSD plots for confined particles before the plateaus. Also, van Hove functions (not shown here) still possess exponential tails at the shortest experimental lag time, 20 ms, suggesting that the experimental time scale is not short enough yet to capture the true diffusive motions of confined particles. Thus, it might be premature to conclude that particles move more slowly within traps due to higher polymer density, as opposed to another possible conclusion that both free and confined particles move at the same speed but the displacements within traps are heavily limited due to the confined geometry.

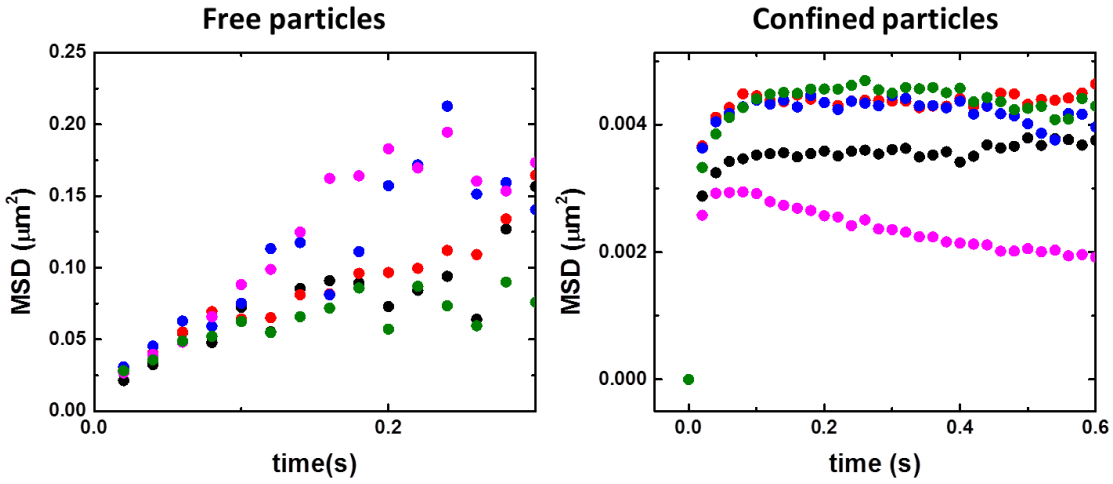

Figure 0.14. MSD plots of free (left) and confined particles (right) in five different spatial positions.

Table 0.4. Local diffusion coefficient and viscosity determined from MSD plots for free and confined particles for 0.7 and 1.5 mol% gel samples.

	0.7 mol%		1.5 mol%	
D ($\mu m^2/s$)	Free	Confined	Free	confined
	0.44 ± 0.08	0.06±0.01	0.24±0.02	0.04±0.01
Est. viscosity (Pa s)	0.05	0.36	0.09	0.53

2.5.7 Distribution of Successive Trap Distances

From the transport property obtained from A^2 values for each composition, global diffusion mechanism seems to be dictated by both travelling distances between traps and caging times which was discussed earlier. Here, we first studied the distribution of successive trap distances to provide an idea how far a single QD travels before it becomes confined again.

Figure 2.15 shows distribution plots of successive trap distances for three different gel compositions, 0.3, 0.7, and 1.5 mol% cross-linker contents. Interestingly, there are very large populations for short distances for all compositions. This length scale is shorter than the characteristic cage sizes that are summarized for each gel composition in Table 2.3 as crossover points, which ranges from 1.4 – 2 pixels (100 – 140 nm). Thus, populations below the red dotted line, which indicates the trap size, suggests that there are frequent recaging events. For now, we are not sure whether these are actual recaging events or artifacts caused by the use of an insufficiently large jump threshold applied to calculations. If focused after the red dotted line, the trend is the breadth of distribution decreases with increasing crosslinker content suggesting that single QDs experience more traps while travelling the same distance at higher crosslinker content. Also, the distribution of 0.3 mol% (black solid circle) shows a plateau-like region or delayed appearance of a bump, and this plateau disappears at 0.7 mol%.

This suggests that single QDs travel farther in more lightly crosslinked gel networks before it gets trapped again, which results in a larger value of A^2.

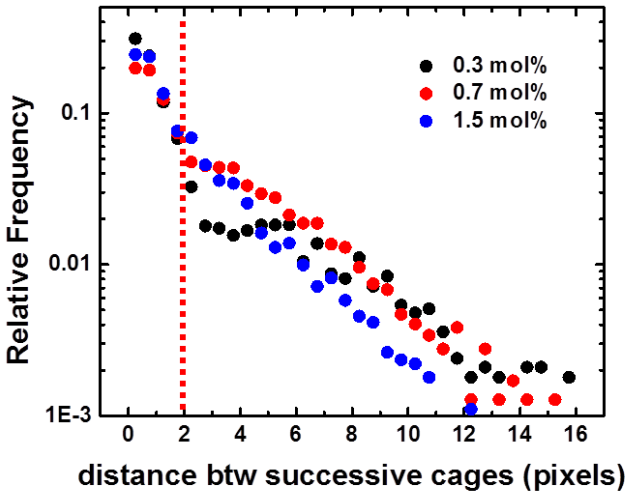

Figure 0.15. Probability distribution of successive trap distances of three different gel compositions, 0.3, 0.7, and 1.5 mol% crosslinker content. The red dotted line indicates the trap size (1.5-2 in pixels) which is determined from the crossover points between Gaussians and exponential tails. Frequency below this line indicates recaging events.

2.5.8 Characteristic Caging Time

The van Hove functions (distribution of single particle displacement) show narrow Gaussian statistics for short displacements and exponential statistics for long displacements in Figure 2.8(a). These two different statistics originate from heterogeneous particle dynamics alternating confined and jumping motions. If there is a characteristic caging time, then one would expect that two different statistics (narrow Gaussian and exponential decay) revert to a broad Gaussian statistics at sufficiently long times. To test whether this happens in our system, we look at long times for van Hove functions. In Figure 2.16, at long lag time of 0.82 and 2

sec, are shown the reversion to Gaussian from exponential decay was observed, which is not quite often, while most van Hove functions for different compositions show exponential statistics until 2 sec. Reversion to Gaussian has been reported from a complex fluid [37, 38] such as colloid gels, where each particle vibrates within a cage formed by neighboring particles, and relaxes moving to the nearest vacant space by thermal energy.

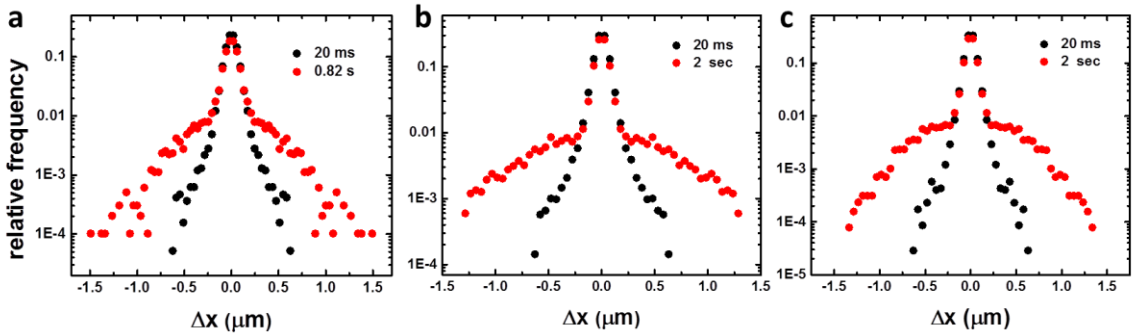

Figure 0.16. Observation of revert to Gaussian from exponential decay at long lag time, 0.82 and 2 sec from QDs moving in (a and b) 0.7 mol% and (c) 1.5 mol% cross-linker content gels with 50 fps frame rates.

Why do we observe the recover to Gaussian when the RT model predicts infinite characteristic caging time? The reason could be explained in many ways. **Firstly**, in the experimental caging time distribution in Figure 2.11 there seems sharp decay for long caging times, which possibly suggests that the actual characteristic caging time in our experiments could be finite value because either particles might be excluded from cages with long caging times or our experimental caging time distribution represents the true energetic distribution (RT model does not predict our system well for long caging times). **Secondly**, according to different emerging times of the reversion to Gaussian (Figure 2.16a and b), samplings of particles are possibly biased from region to region. Some regions do not sample particles

experiencing long caging times, which could cause a finite characteristic caging time during observation. **Finally**, in the case of a system with an infinite characteristic caging time, since jumping displacements are rare events, Poisson distribution can describe the exponential distribution of magnitude of jumping displacement for short lag time when the number of jumping events is quite limited. However, if we wait for a long time even though it cannot be longer than infinite characteristic caging time, there always exist particles experiencing shorter caging times than experimental time scale, such as region *A* in Figure 2.17. These particles experiencing short caging times allow for the sampling of more jumping events leading exponential decay to be approximated to Gaussian at some point. Of course, there are also many particles experiencing longer caging times than τ, which cannot be sampled for jumping events, but it does not matter as long as we can sample jumping events from region *A*. Particles experiencing longer caging times in region *B* contribute to narrow Gaussian statistics for short displacements which never disappears due to infinite characteristic caging time. The conclusion is that the reversion of Gaussian statistics for distribution of jumping displacements does not require sampling of all particles, while, for the recover to the linear relationship of MSD with lag time, it requires to sample all displacements of particles at a specific lag time when there are many particles still trapped, which suppress the MSD values.

Thus, it seems premature to conclude whether the characteristic caging time exists in our system. Instead, we leave it as open questions how can we experimentally define the characteristic caging time in our system?, and what time scale represents a long enough experimental time window to observe the reversion to Gaussian from exponential decay in a system with infinite characteristic caging time?

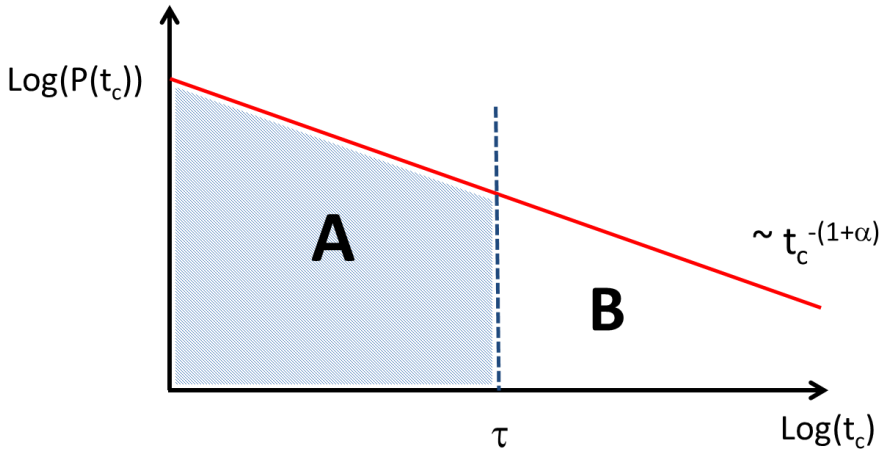

Figure 0.17. Caging time distribution of the RT model. τ is the experimental lag time. In shaded region A, caging times are shorter than experimental lag time where jumping events can be observed, while in region B where caging time is longer than τ, jumping events cannot be observed within experimental lag time.

2.6 Conclusion

We have characterized the motion of single quantum dot probes as a means to study structural heterogeneity in polyacrylamide hydrogels. Over the five-fold range in crosslinker content considered, the probes were found to exhibit sub-diffusive motion at all gel compositions, though with increasingly restricted motion as crosslinking became more extensive. Analyses of mean-square displacements showed clear qualitative signatures of sub-diffusion, but otherwise were found not to be a robust means for characterizing motion in these materials. Interestingly, van Hove correlation functions showed that particles in each gel undergo diffusive motion on scales up to ~ 100 – 140 nm, suggesting the presence of regions with lower-density in this size regime that allow for free motion locally. However, they also showed exponential tails for larger displacements, indicating the presence of barriers between

neighboring trap sites that cause long-range motion to be dominated by relatively rare escape events. The characteristic length scale λ over which particles had moved was found to increase with lag time according to a power-law with an exponent of $\beta \approx 0.33$. In addition, the distributions of particle caging times were found to be well described, at least for relatively short caging times, by a simple random trap (RT) model with an exponential distribution of trap energies, and characteristic energies ranging from ~ 1 to 3 times thermal energy with increasing crosslink density. These results are largely consistent with prior interpretations of scattering and bulk permeability measurements on samples with similar compositions, but provide new insights into the distribution of micro-environments within these inherently heterogeneous materials. Especially if extended to multi-color imaging of several different QD probe sizes, we anticipate that this experimental method has the potential to provide a wealth of information on the structures of a wide variety of networks with nanometer-scale porosities, and should yield sensitive tests of more refined models for the landscape of trap energies within these materials.

2.7 References

1. Bastide, J. and L. Leibler, *Large-scale heterogeneities in randomly cross-linked networks.* Macromolecules, 1988. ***21***(8): p. 2647-2649.

2. Lutolf, M.P., *Biomaterials: Spotlight on hydrogels.* Nat Mater, 2009. ***8***(6): p. 451-453.

3. Drury, J.L. and D.J. Mooney, *Hydrogels for tissue engineering: scaffold design variables and applications.* Biomaterials, 2003. ***24***(24): p. 4337-4351.

4. Hoare, T.R. and D.S. Kohane, *Hydrogels in drug delivery: Progress and challenges.* Polymer, 2008. ***49***(8): p. 1993-2007.

5. Annaka, M., et al., *Preparation of Comb-Type N-Isopropylacrylamide Hydrogel Beads and Their Application for Size-Selective Separation Media.* Biomacromolecules, 2003. ***4***(2): p. 395-403.

6. Weiss, N. and A. Silberberg, *Inhomogeneity of polyacrylamide gel structure from permeability and viscoelasticity.* British Polymer Journal, 1977. ***9***(2): p. 144-150.

7. Richards, E.G. and C.J. Temple, *Some Properties of Polyacrylamdie Gels.* Nature Physical Science, 1971. ***230***: p. 92-96.

8. Valentine, M.T., et al., *Investigating the microenvironments of inhomogeneous soft materials with multiple particle tracking.* Physical Review E, 2001. **64**(6): p. 061506.

9. Fawcett, J.S. and C.J.O.R. Morris, *Molecular-sieve chromatography of proteins on granulated polyacrylamide gels.* Separation science, 1966. ***1***: p. 9-26.

10. Zhang, J., C.R. Daubert, and E.A. Foegeding, *Characterization of polyacrylamide gels as an elastic model for food gels.* Rheologica Acta, 2005. ***44***(6): p. 622-630.

11. Bansil, R. and M.K. Gupta, *EFFECT OF VARYING CROSSLINKING DENSITY ON POLYACRYLAMIDE GELS.* Ferroelectrics, 1980. ***30***(1-4): p. 63-71.

12. Scalfani, V.F. and T.S. Bailey, *Access to Nanostructured Hydrogel Networks through Photocured Body-Centered Cubic Block Copolymer Melts.* Macromolecules, 2011. ***44***(16): p. 6557-6567.

13. Chrambach, A. and D. Rodbard, *Polyacrylamide Gel Electrophoresis.* Science, 1971. ***172***(3982): p. 440-451.

14. Yeung, T., et al., *Effects of substrate stiffness on cell morphology, cytoskeletal structure, and adhesion.* Cell Motility and the Cytoskeleton, 2005. ***60***(1): p. 24-34.

15. Pelham, R.J. and Y.-l. Wang, *Cell locomotion and focal adhesions are regulated by substrate flexibility.* Proceedings of the National Academy of Sciences, 1997. ***94***(25): p. 13661-13665.

16. Hecht, A.M., R. Duplessix, and E. Geissler, *Structural inhomogeneities in the range 2.5-2500 Å in polyacrylamide gels.* Macromolecules, 1985. ***18***(11): p. 2167-2173.

17. Mallam, S., et al., *Scattering and Swelling Properties of Inhomogeneous Polyacrylamide Gels.* Macromolecules, 1989. ***22***(8): p. 3356-3361.

18. Shibayama, M., *Spatial inhomogeneity and dynamic fluctuations of polymer gels.* Macromolecular Chemistry and Physics, 1998. ***199***(1): p. 1-30.

19. Hsu, T.P. and C. Cohen, *Observations on the Structure of a Polyacrylamide-Gel from Electron-Micrographs.* Polymer, 1984. ***25***(10): p. 1419-1423.

20. Ruchel, R., R. Steere, and E. Erbe, *Tansmission electron microscopic observation of freeze etched polyacrylamide gels.* Journal of Chromatography, 1978. ***166***: p. 563.

21. Holmes, D.L. and N.C. Stellwagen, *Estimation of polyacrylamide gel pore size from Ferguson plots of linear DNA fragments. II. Comparison of gels with different crosslinker concentrations, added agarose and added linear polyacrylamide.* ELECTROPHORESIS, 1991. **12**(9): p. 612-619.

22. Xue, J.Z., et al., *Nonergodicity and light scattering from polymer gels.* Physical Review A, 1992. **46**(10): p. 6550-6563.

23. Saxton, M.J., *Single-particle tracking: connecting the dots.* Nat Meth, 2008. **5**(8): p. 671-672.

24. Schmidt, T., et al., *Imaging of single molecule diffusion.* Proceedings of the National Academy of Sciences of the United States of America, 1996. **93**(7): p. 2926-2929.

25. Weigel, A.V., et al., *Ergodic and nonergodic processes coexist in the plasma membrane as observed by single-molecule tracking.* Proceedings of the National Academy of Sciences, 2011. **108**(16): p. 6438-6443.

26. Yildiz, A., et al., *Myosin V Walks Hand-Over-Hand: Single Fluorophore Imaging with 1.5-nm Localization.* Science, 2003. **300**(5628): p. 2061-2065.

27. Saxton, M.J. and K. Jacobson, *SINGLE-PARTICLE TRACKING:Applications to Membrane Dynamics.* Annual Review of Biophysics and Biomolecular Structure, 1997. **26**(1): p. 373-399.

28. Haramagatti, C.R., et al., *Diblock copolymer membranes investigated by single-particle tracking.* Physical Chemistry Chemical Physics. **13**(6): p. 2278-2284.

29. McCain, K.S., D.C. Hanley, and J.M. Harris, *Single-Molecule Fluorescence Trajectories for Investigating Molecular Transport in Thin Silica Sol−Gel Films.* Analytical Chemistry, 2003. **75**(17): p. 4351-4359.

30. Fu, Y., et al., *Single Molecule Spectroscopy Studies of Diffusion in Mesoporous Silica Thin Films.* The Journal of Physical Chemistry B, 2006. **110**(18): p. 9164-9170.

31. Roeffaers, M.B.J., et al., *Spatially resolved observation of crystal-face-dependent catalysis by single turnover counting.* Nature, 2006. **439**(7076): p. 572-575.

32. Schultz, K.M., et al., *Gelation of Covalently Cross-Linked PEG−Heparin Hydrogels.* Macromolecules, 2009. **42**(14): p. 5310-5316.

33. He, K., et al., *Diffusive Dynamics of Nanoparticles in Arrays of Nanoposts.* ACS Nano, 2013. **7**(6): p. 5122-5130.

34. Dickson, R.M., et al., *Three-Dimensional Imaging of Single Molecules Solvated in Pores of Poly(acrylamide) Gels.* Science, 1996. **274**(5289): p. 966-968.

35. Elliott, L.C.C., et al., *Trajectory analysis of single molecules exhibiting non-Brownian motion.* Physical Chemistry Chemical Physics. **13**(10): p. 4326-4334.

36. Wong, I.Y., et al., *Anomalous Diffusion Probes Microstructure Dynamics of Entangled F-Actin Networks.* Physical Review Letters, 2004. **92**(17): p. 178101.

37. Wang, B., et al., *Anomalous yet Brownian.* Proceedings of the National Academy of Sciences, 2009. **106**(36): p. 15160-15164.

38. Gao, Y. and M.L. Kilfoil, *Intermittent and spatially heterogeneous single-particle dynamics close to colloidal gelation.* Physical Review E, 2009. **79**(5): p. 051406.

39. Chaudhuri, P., L. Berthier, and W. Kob, *Universal Nature of Particle Displacements close to Glass and Jamming Transitions.* Physical Review Letters, 2007. **99**(6): p. 060604.

40. Chaudhuri, P., et al., *A random walk description of the heterogeneous glassy dynamics of attracting colloids.* Journal of Physics-Condensed Matter, 2008. **20**(24): p. 244126.

41. Saltzman, E.J. and K.S. Schweizer, *Large-amplitude jumps and non-Gaussian dynamics in highly concentrated hard sphere fluids.* Physical Review E, 2008. **77**(5): p. 051504.

42. Bouchaud, J.-P. and A. Georges, *Anomalous diffusion in disordered media: Statistical mechanisms, models and physical applications.* Physics Reports, 1990. **195**(4–5): p. 127-293.

43. Havlin, S. and D. Ben-Avraham, *Diffusion in disordered media.* Advances in Physics, 2002. **51**(1): p. 187-292.

44. Haus, J.W. and K.W. Kehr, *Diffusion in regular and disordered lattices.* Physics Reports, 1987. **150**(5–6): p. 263-406.

45. Montroll, E.W. and G.H. Weiss, *Random Walks on Lattices .2.* Journal of Mathematical Physics, 1965. **6**(2): p. 167.

46. Monthus, C. and J.P. Bouchaud, *Models of traps and glass phenomenology.* Journal of Physics a-Mathematical and General, 1996. **29**(14): p. 3847-3869.

47. Heitjans, P. and J. Karger, eds. *Diffusion in condensed matter*. 2005.

48. Berlin, Y.A., L.D.A. Siebbeles, and A.A. Zharikov, *Thermally activated diffusion along one-dimensional chains with energetic disorder: analysis of computer simulation data.* Chemical Physics Letters, 1997. **276**(5–6): p. 361-370.

49. Bässler, H., *Localized states and electronic transport in single component organic solids with diagonal disorder.* physica status solidi (b), 1981. **107**(1): p. 9-54.

50. Drazer, G., M. Rosen, and D.H. Zanette, *Anomalous transport in activated carbon porous samples: power-law trapping-time distributions.* Physica A: Statistical Mechanics and its Applications, 2000. **283**(1–2): p. 181-186.

51. Frauenfelder, H., S. Sligar, and P. Wolynes, *The energy landscapes and motions of proteins.* Science, 1991. **254**(5038): p. 1598-1603.

52. Dahan, M., et al., *Diffusion Dynamics of Glycine Receptors Revealed by Single-Quantum Dot Tracking.* Science, 2003. **302**(5644): p. 442-445.

53. Holtzer, L., T. Meckel, and T. Schmidt, *Nanometric three-dimensional tracking of individual quantum dots in cells.* Applied Physics Letters, 2007. **90**(5): p. 053902-3.

54. Murcia, M.J., et al., *Design of Quantum Dot-Conjugated Lipids for Long-Term, High-Speed Tracking Experiments on Cell Surfaces.* Journal of the American Chemical Society, 2008. **130**(45): p. 15054-15062.

55. Tada, H., et al., *In vivo Real-time Tracking of Single Quantum Dots Conjugated with Monoclonal Anti-HER2 Antibody in Tumors of Mice.* Cancer Research, 2007. **67**(3): p. 1138-1144.

56. Sudeep, P.K., et al., *Monodisperse Oligo(phenylene vinylene) Ligands on CdSe Quantum Dots: Synthesis and Polarization Anisotropy Measurements.* Journal of the American Chemical Society, 2008. ***130***(8): p. 2384-2385.

57. Dabbousi, B.O., et al., *(CdSe)ZnS Core-Shell Quantum Dots: Synthesis and Characterization of a Size Series of Highly Luminescent Nanocrystallites.* The Journal of Physical Chemistry B, 1997. ***101***(46): p. 9463-9475.

58. Yu, W.W., et al., *Experimental Determination of the Extinction Coefficient of CdTe, CdSe, and CdS Nanocrystals.* Chemistry of Materials, 2003. ***15***(14): p. 2854-2860.

59. Dasgupta, B.R. and D.A. Weitz, *Microrheology of cross-linked polyacrylamide networks.* Physical Review E, 2005. **71**(2): p. 021504.

60. Susumu, K., B.C. Mei, and H. Mattoussi, *Multifunctional ligands based on dihydrolipoic acid and polyethylene glycol to promote biocompatibility of quantum dots.* Nat. Protocols, 2009. **4**(3): p. 424-436.

61. Uyeda, H.T., et al., *Synthesis of Compact Multidentate Ligands to Prepare Stable Hydrophilic Quantum Dot Fluorophores.* Journal of the American Chemical Society, 2005. **127**(11): p. 3870-3878.

62. Mei, B.C., et al., *Polyethylene glycol-based bidentate ligands to enhance quantum dot and gold nanoparticle stability in biological media.* Nat. Protocols, 2009. **4**(3): p. 412-423.

63. Crocker, J.C. and D.G. Grier, *Methods of Digital Video Microscopy for Colloidal Studies.* Journal of Colloid and Interface Science, 1996. **179**(1): p. 298-310.

64. *MATLAB codes are available at http://www.physics.georgetown.edu/matlab/index.html.*

65. Steven, F.L. and A.O. Mark, *Brightening, Blinking, Bluing and Bleaching in the Life of a Quantum Dot: Friend or Foe?* ChemPhysChem, 2009. **10**(13): p. 2174-2191.

66. Scalas, E., *The application of continuous-time random walks in finance and economics.* Physica A: Statistical Mechanics and its Applications, 2006. **362**(2): p. 225-239.

67. Cheng, N.-S., *Formula for the Viscosity of a Glycerol−Water Mixture.* Industrial & Engineering Chemistry Research, 2008. **47**(9): p. 3285-3288.

68. Pons, T., et al., *Hydrodynamic Dimensions, Electrophoretic Mobility, and Stability of Hydrophilic Quantum Dots.* The Journal of Physical Chemistry B, 2006. ***110***(41): p. 20308-20316.

69. Kizilay, M.Y. and O. Okay, *Effect of hydrolysis on spatial inhomogeneity in poly(acrylamide) gels of various crosslink densities.* Polymer, 2003. ***44***(18): p. 5239-5250.

70. Savin, T. and P.S. Doyle, *Statistical and sampling issues when using multiple particle tracking.* Physical Review E, 2007. **76**(2): p. 021501.

71. Calvet, D., J.Y. Wong, and S. Giasson, *Rheological Monitoring of Polyacrylamide Gelation: Importance of Cross-Link Density and Temperature.* Macromolecules, 2004. **37**(20): p. 7762-7771.

72. Barkai, E., Y. Garini, and R. Metzler, *Strange kinetics of single molecules in living cells.* Physics Today, 2012. **65**(8): p. 29-35.

73. Burov, S. and E. Barkai, *Time Transformation for Random Walks in the Quenched Trap Model.* Physical Review Letters, 2011. **106**(14): p. 140602.

CHAPTER 3

ASSEMBLY OF Quantum Dot RINGS AT THE AIR/WATER INTERFACE BY 2-D PICKERING EMULSIONS[2]

3.1 Introduction

Semiconductor and metal nanoparticles (NPs) are attractive building blocks for fabricating nano- and microscale structures, which are important components of photonic, electronic and magnetic devices for sensing, optical, and other applications. [1-7] In many cases, the ability to assemble NPs into ordered structures on substrates is critically important. For example, Keng *et al*. assembled polymer-coated ferromagnetic cobalt NPs into 1-D and 2-D structures, enabled by the inherent dipole moment of the NPs. [8] Kim *et al*. employed flow-coating to produce well-aligned stripe and grid patterns of quantum dots (QDs), [2] where a QD solution is loaded and trapped in a confined geometry by capillary forces, and translation of an underlying substrate affords QD deposition along the contact line during solvent evaporation. Numerous approaches have been reported to fabricate patterns of nano- or microscale particles by template-based assembly. [4, 5, 9-12] However, self- or directed-assembly methods that eliminate the need for template fabrication remain of interest for assembling NPs over large areas in a simple fashion.

[2] Reprinted and adapted from the manuscript submitted to ACS Applied Materials and Interfaces.

The formation of NP rings has attracted particular attention due to their suitability as optical and electronic resonators. [13-17] Chen *et al*. demonstrated the controlled formation of 2-D periodic arrays of nanorings from CdSe QDs by introducing an aqueous solution of microspheres and QDs onto a glass substrate. [1] QDs became confined to the meniscus of the microspheres during evaporation, leading to QD rings by capillary forces. Boker *et al.* produced well-ordered hexagonal patterns of QDs assembled at an oil/water interface. [18] Evaporative cooling of a volatile polymer solution containing QDs produced micron-sized water droplets on the polymer surface, giving 'breath figures' in which the QDs segregate to the polymer solution/water droplet interface. Khanal *et al.* demonstrated the formation of rings of PS-functionalized Au nanorods using a similar breath figure technique. [19]

In this chapter, we present a simple solution-based self-assembly method that affords 2-D QD ring structures. This began with the unanticipated formation of QD rings on the surface of water droplets containing PEGylated CdSe/ZnS core/shell QDs on borosilicate coverslips. Further investigation revealed that this behavior arose due to the presence of surface-active impurities present on the glass surface, and led to experiments showing that such assemblies can be achieved by introducing a suitable concentration of insoluble surfactant. We speculate that the surfactant molecules form islands at the air/water interface (where gas (G) and liquid expanded (LE) phases coexist) followed by QD adsorption to the three phase interfacial line of the islands, in a process driven by a reduction in interfacial energy. The areal density of surfactant molecules proved critical to the successful formation of QD rings, and the rings could be transferred to other substrates by dip-coating.

3.2 Experimental

3.2.1 Water Soluble CdSe/ZnS Core/Shell Quantum Dots.

CdSe/ZnS core/shell QDs were synthesized according to literature methods. [20-22] Two QD samples were used, having 4 and 9 nm diameter as determined by UV-Vis absorption [23] and TEM. Ligand exchange was conducted on the QDs, converting the surface functionality to polyethylene glycol (Mn = 600) with a dihydrolipoic acid (DHLA) binding group (PEG-DHLA). [24] Briefly, 1 – 2 mg of TOPO- or oleic acid- capped QDs, 50 – 100 mg of excess DHLA-PEG600 ligand, and 0.3 – 0.4 mL of methanol were placed in a 4 mL vial and degassed. This mixture was stirred overnight at 70 ^{o}C until the solution became clear, then cooled to room temperature and precipitated by adding hexane and chloroform. The supernatant was removed, and water was added to dissolve the QDs. The aqueous QD solution was purified by passing through a centrifugal filter membrane (MWCO = 100 kDa) in RO water.

3.2.2 Synthesis of DHLA-PEG600.

DHLA-PEG600 ligand was synthesized by following literature methods. [24, 25] Thioctic acid (5.0 g, 24 mmol), poly(ethylene glycol) (MW = 600, 145 g, 242 mmol), a catalytic amount of 4-(dimethylamino)-pyridine (890 mg, 7.3 mmol), and CH_2Cl_2 (240 mL) were combined in a flask and degassed with N_2. The mixture was cooled to 0 ^{o}C in an ice bath, and a solution of dicyclohexylcarbodiimide (6.5 g, 31 mmol) in CH_2Cl_2 (20 mL) was added dropwise. The mixture was stirred overnight at room temperature. The precipitate was filtered over a plug of Celite, and the residue was mixed with an aqueous sodium bicarbonate solution, and extracted with ethyl acetate (3 times). The combined organic phase was dried over

$MgSO_4$, filtered, and evaporated to give a yellow oil. This oil was purified by column chromatography on silica gel (chloroform/methanol 95:5), and the product recovered as a yellow oil (~ 60 %). Sodium borohydride (13.8 mmol) in a 1:4 ethanol/water (55 mL) was used to reduce the disulfide, giving PEG-DHLA.

3.2.3 Octadecyltrichlorosilane (OTS) Coating on Coverslips (Borosilicate Micro Cover Glasses).

A coverslip (VWR® micro cover glasses, No. 1.5, catalog number: 48393-194) was sonicated in toluene for 20 min, and subjected to UV/ozone treatment for 30 min. The cleaned coverslip was immersed into 0.1 v/v% OTS in toluene, and the solution was stirred for 1 hr. Then, OTS treated coverslip was washed with toluene and isopropanol several times. To reduce the water contact angle of OTS treated substrates to ~35^o, it was exposed to UV/ozone for ~ 6 min resulting in partial oxidization of OTS layer.

3.2.4 Quantum Dot Ring Formation on Substrates.

A droplet of 0.4 wt% aqueous solution of acrylamide, containing PEGylated QDs (~1 nM), was placed on various substrates, such as coverslip, silicon wafer, TEM grid, OTS treated glass, and soda-lime glass slide (1 mm thick). Among all of these substrates, QD rings formed only on the glass coverslips. The coverslips were used as received with brief rinsing with water.

3.2.5 Quantum Dot Ring Deposition and Alignment by Dip-Coating.

A 0.4 wt% aqueous solution of acrylamide, containing PEGylated QDs (~1 nM), was filled in a cylindrical chamber, and a coverslip (22 mm x 50 mm) was immersed in a solution. After ~15 min, QD rings formed at the interface were deposited on a coverslip by dip-coating with a continuous withdrawal rate of 1 μm/s using servo motor (Parker Daedal, Parker Hannifin Corp., Cleveland, OH). The alignment of the rings was achieved by dip-coating in a controlled manner, with 1 min stopping time in between 2 mm/s withdrawals steps. The movement of substrates was controlled at a computer interface with LabView (National Instruments, Austin, TX) software.

3.3 Results and Discussion

3.3.1 Formation of Quantum Dot Rings at the Air/Water Interface

The unexpected observation of 2-D QD assembly into rings at the air/water interface occurred when a droplet of aqueous solution containing ~ 0.4 wt% acrylamide and ~ 1 nM QDs was placed onto a borosilicate coverslip substrate. The fluorescence micrographs of Figures 3.1a and b represent typical examples of QD rings formed at the air/water interface near the contact line of the droplet. In contrast, Figure 3.1c shows a network morphology of QDs on top of a droplet. In Figures 3.1a and b, QD rings in the center of the images are in focus, while the rings in the upper and lower regions are out of focus; this is caused by the curvature of the droplet near the contact line. The QD rings were observed near the edge of the droplet of this solution during evaporation, rather than on the whole of the droplet. The observed QD rings covered a range of sizes, from hundreds of nanometers to ~10 microns in

diameter. Two different QDs in size, 4 and 10 nm, were used to make rings as shown in Figure 3.2.

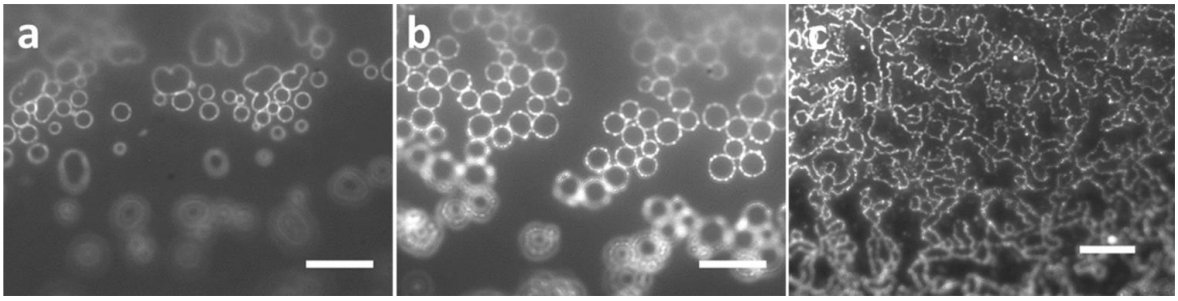

Figure 0.1. (a and b) Fluorescence microscope images of QD rings formed at the edge of the droplet (scale bar = 10 μm); (c) QD network formed on top of the droplet surface (scale bar = 20 μm).

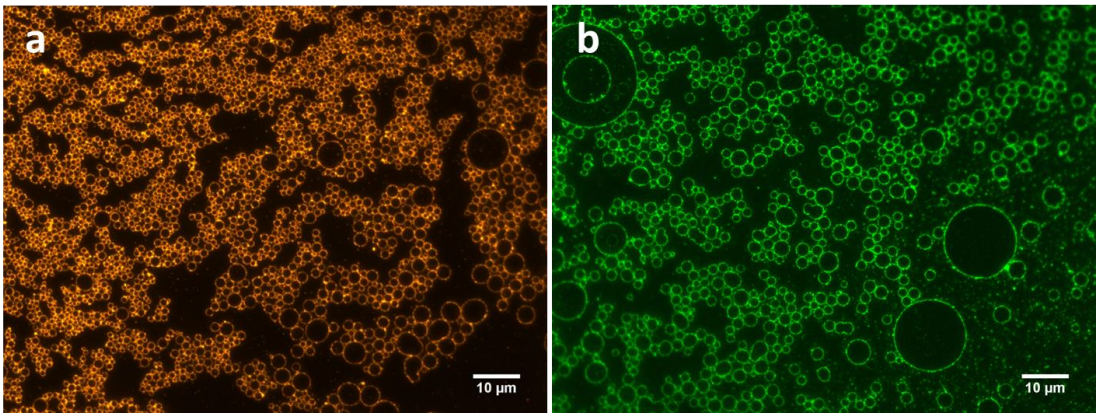

Figure 0.2. QD rings formed from two QDs different in sizes, 4 nm (a) and 10 nm (b), respectively.

3.3.2 Characterization of Quantum Dot Rings

Figure 3.3a shows a fluorescence microscope image of QD rings deposited on the coverslip substrate upon evaporation of water and recession of the contact line. The solid

arrow denotes the contact line, and the dashed arrow the receding direction. The upper left portion of the image shows QD rings after deposition; in the lower right of the image, no QD rings are visible because the rings are out of focus (the substrate is in focus). After deposition, the QD rings were characterized by electron microscopy and atomic force microscopy (AFM). Figures 3.3 (b-d) show scanning electron microscopy (SEM) and AFM images of the QD rings. The SEM image of Figure 3.3b shows an easily recognized ring with a continuous rim consisting of QDs. The AFM image of Figure 3.3d shows a discrete circular pattern, with a height corresponding to the QD diameter of ~ 5 nm, while the phase image in Figure 3.3c indicates the presence of material, likely the ring template-forming material, inside the rings. In Figure 3.4, AFM height analysis of a single QD ring indicates that the height of inside the ring is higher than substrate suggesting that some materials occupy the inside of the ring, which is corresponding to the AFM phase image in Figure 3.3c.

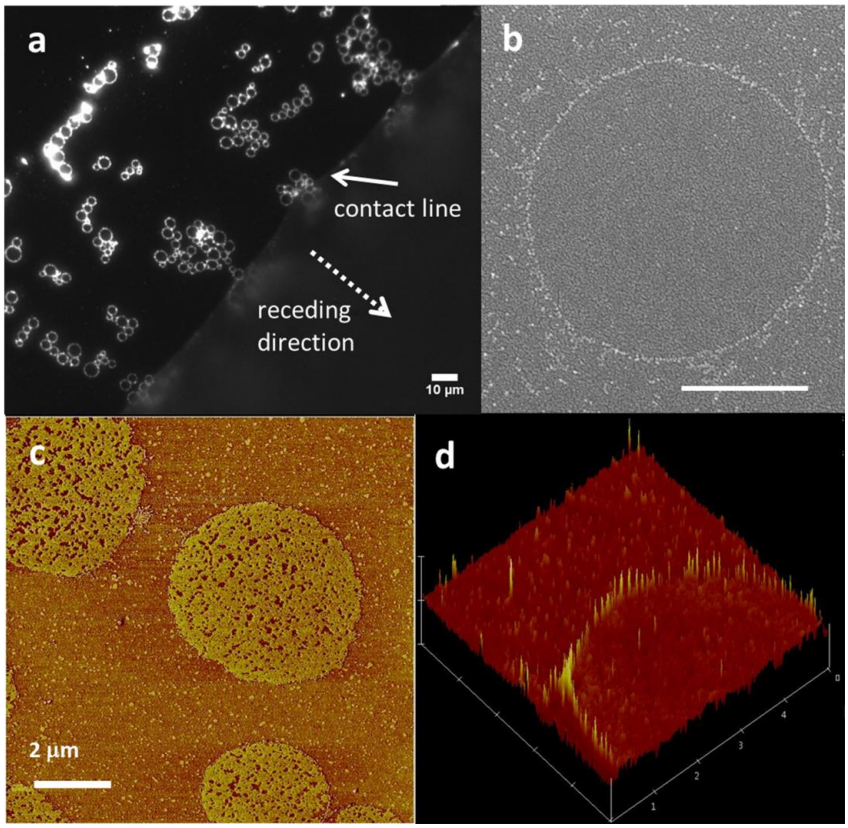

Figure 0.3. (a) Fluorescence microscope image of QD rings deposited on borosilicate glass as the contact line recedes: the solid arrow indicates the contact line and the dotted one the receding direction; (b) SEM image of a QD ring (scale bar = 1 μm); (c) AFM phase image; (d) 3-D AFM height image: the lateral dimension is 5 μm ×5 μm and vertical dimension is ± 5 nm.

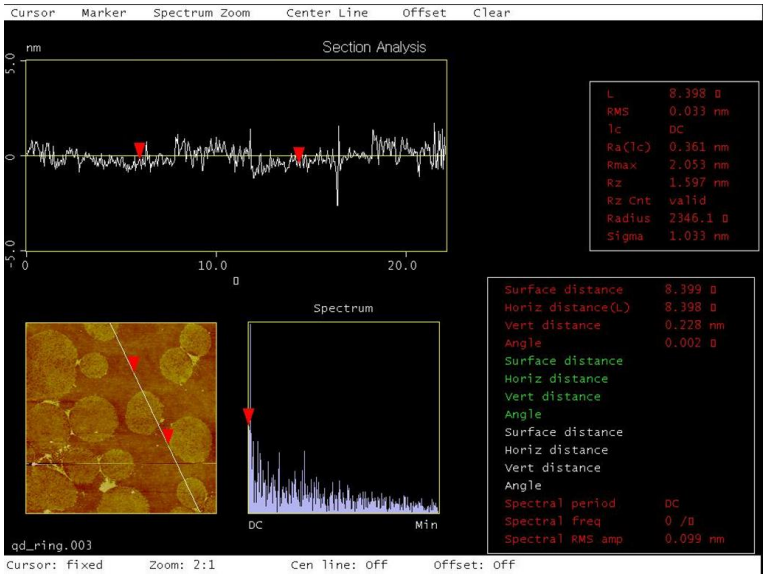

Figure 0.4. AFM height analysis of a single QD ring indicating that the height inside the ring is higher than the substrate (outside the ring).

3.3.3 Assembly of Surfactant Islands

Interestingly, attempts to form QD rings on numerous other substrates (TEM grids, Si wafers, or other glass substrates) failed. Indeed, we were able to reproduce QD ring formation from the droplets only on the glass coverslips used in our initial experiments. The water contact angle of these coverslip was higher (~ 35^{o}) than the other glass substrates tested (~ 10^{o}). We suspect this difference in contact angle reflects the presence of organic impurities on the untreated borosilicate coverslip surfaces, as described by Sumner.[26] Extensive cleaning (solvent washing, plasma, or UV/ozone cleaning) of these coverslips reduced the water contact angle to $<10^{o}$, but this treatment precluded the formation of QD rings. Thus, it seems that organic impurities are key to QD ring formation, rather than the acrylamide, though we note the possibility for acrylamide to function as a surfactant as well.[27] Indeed, in some cases, the QD rings formed on the coverslips when acrylamide was excluded from the

experiments as shown in Figure 3.5. This variability of QD ring formation is also found in the presence of acrylamide, and this variability may reflect different amounts of impurities on the coverslips in each trial.

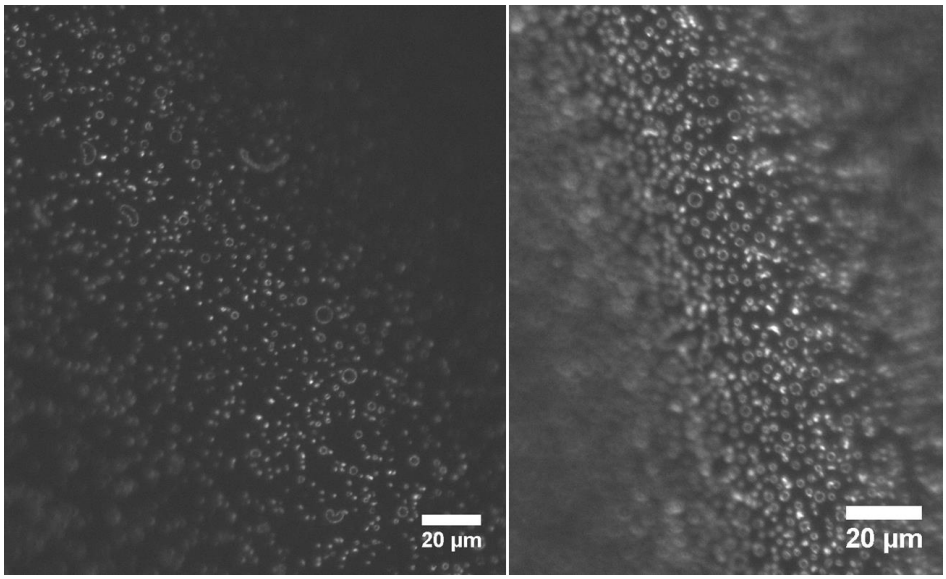

Figure 0.5. QD rings form on untreated coverslips in the absence of acrylamide.

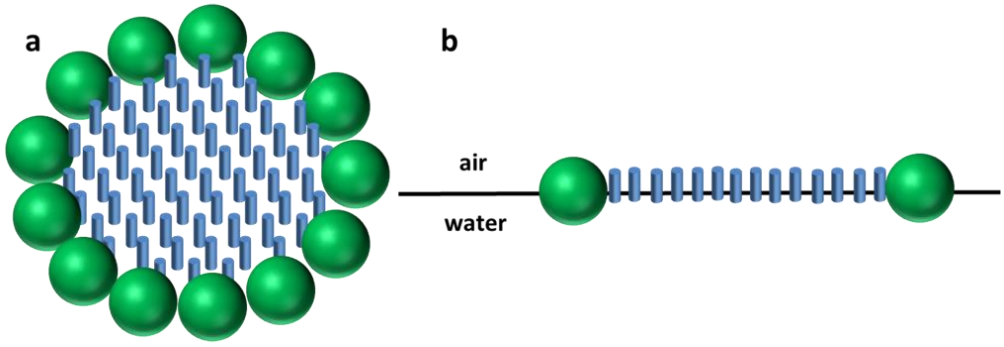

Figure 0.6. Schematic of 2-D Pickering emulsions at the air/water interface. (a) Top view and (b) side view of 2-D Pickering emulsions where green dots refer to QDs and blue rods surface active impurities.

Thus, a further investigation was undertaken, with the objective of producing QD rings on substrates other than the more hydrophobic commercial coverslips. Attempts to form QD rings on OTS treated coverslips (CA ~90^{o}) and oxidized OTS-treated coverslip (CA ~35^{o}) both failed, suggesting that CA is not the key determining factor in QD ring formation. We speculate that the impurities from the coverslip are surface active, and leach from the surface to the air/water interface, followed by the adsorption of QDs surrounding the impurity islands that can be considered as a 2-D Pickering emulsion, as depicted in Figure 3.6.[28] Motivated by this hypothesis, we examined the effect of added surfactant, such as myristic acid (MA), which is known to form islands at the air/water interface due to coexistence of gas (G) and liquid expanded (LE) phases. [29-31] Solutions of MA were first prepared in chloroform at concentrations from 0.1 to 50 μM, then 10 μL of a QD solution (~1 nM in water) was placed on OTS treated coverslips (exposed with UV-ozone for partial oxidation) followed by a 0.5 μL drop of surfactant stock solution that spread at the air/water interface. Figure 3.7a shows fluorescence microscope images of QD rings formed from experiments having a 0.5 μM surfactant stock solution. QD ring formation occurred quickly in these experiments (~ 1 min), suggesting fast adsorption kinetics of QD to the interface. MA concentration proved important, as no ring formation was observed at values substantially above or below ~0.5 μM. Assuming the MA to spread uniformly over the droplet surface, this corresponds to an area of ~ 10^4 Å^2/molecule, which is far greater than the value of ~200-400 Å^2/molecule reported for the G-LE transition in MA.[31, 32] Thus, while the density is too low for G-LE coexistence in the absence of QDs, we speculate that adsorption of QDs to the edges of surfactant islands stabilizes LE droplets. Once QD rings form on the surface of droplets, they change shape as water evaporates, due to the decrease in the surface area, while QD rings formed at a flat

air/water interface do not show shape deformation over time (Figure 3.7b). As seen in Figure 3.7, although QD rings formed with MA were found to appear less organized than those in Figures 3.1 (a and b), the formation of QD rings in the presence of myristic acid strongly support our hypothesis that surface active impurities from the coverslip were responsible for the formation of QD rings. Whether other types of nanoparticles (metallic, magnetic, etc) could participate in such ring formation is an open question and a topic of future investigation, although we think it should be a general strategy given proper ligands that allow adsorption of nanoparticles at the edge of surfactant domains.

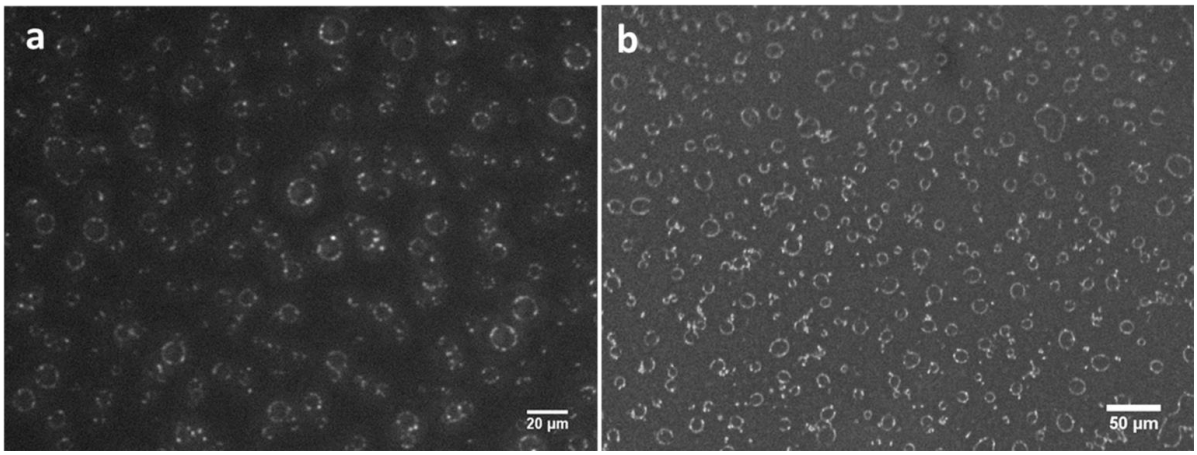

Figure 0.7. Fluorescence microscope images of QD rings formed in the presence of myristic acid at the air/water interface. (a) QD rings on top of a droplet surface and (b) QD rings formed on a flat air/water interface. (Scale bar = 20 μm).

However, in case of the flat surface, it was more difficult to observe the formation of QD rings, which is not explained yet. Also, QD rings were observed from two different concentrations of MA stock solutions, ~1 and ~50 mM, with non-uniform distribution of QD rings at the interface as shown in Figure 3.8. Thus, we were determined to find out the areal

density of surfactant molecules over the area where QD rings are formed. Since we cannot assume the uniform spreading of surfactant molecules to directly calculate the areal density per molecule, the areal coverage, instead, of QD rings over the yellow square in Figure 3.8 is compared with areal coverage in Figure 3.7a, which are 0.16 and 0.06, respectively. The difference in these two values could come from the measurement errors or the possible existence of surfactant islands which is invisible due to no QDs around them. Given these possible errors, the areal densities of both cases seem to be similar, suggesting that the formation of QD rings requires a certain areal density of surfactant molecules.

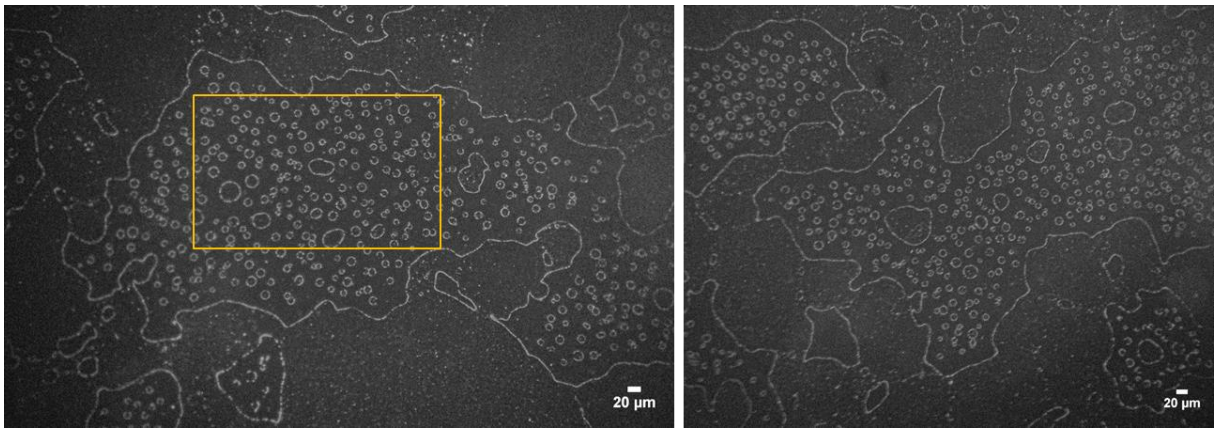

Figure 0.8. Non-uniform distribution of QD rings over the area of flat interface. The areal coverage of QD rings were calculated from inside the yellow square to compare it with the areal density of surfactant molecules in Figure 3.7a.

3.3.4 Deposition & Alignment of Quantum Dot Rings

Beyond the formation of individual QD rings, we found that the rings could be aligned over a large area (~cm^2) by dip-coating onto untreated coverslips (Figure 3.9). For example, an aqueous acrylamide solution (~0.4 wt %) containing QDs was filled in a chamber with a

circular opening, and a coverslip was immersed at an angle of ~35-45^{o}. Figure 3.9a shows a fluorescence microscope image of deposited QD rings after dip-coating, with a continuous withdrawal rate of 1 μm/s at an angle of ~ 35^{o}. Alignment of the rings was accomplished by implementing a 1 minute stopping time between 0.5 second withdrawal steps at 2 mm/s at an angle of ~45^{o}. In Figure 3.9b, the pulling direction of the substrate is indicated by the arrow, and QD rings were aligned on the substrate at the initial contact line, with the quick slip motion of the substrate, to give lines of rings along the contact line. In Figure 3.10, a series of images of aligned QD rings is shown with numbers indicating n-th pulling of the substrate. From the 5th pull, QD rings were consistently aligned along the contact line. Pulling direction of a substrate was towards right, and there exist aggregates of QDs deposited on the right side of QD ring alignments due to water evaporation during the stopping time. Interestingly, the aligned rings in Figure 3.9(b) are rather uniform in size compared to those in Figure 3.2. However, we note that in many cases the sizes of aligned rings are more broadly distributed. This demonstrates a very simple and effective method of QD ring deposition over a large area (~cm^{2}).

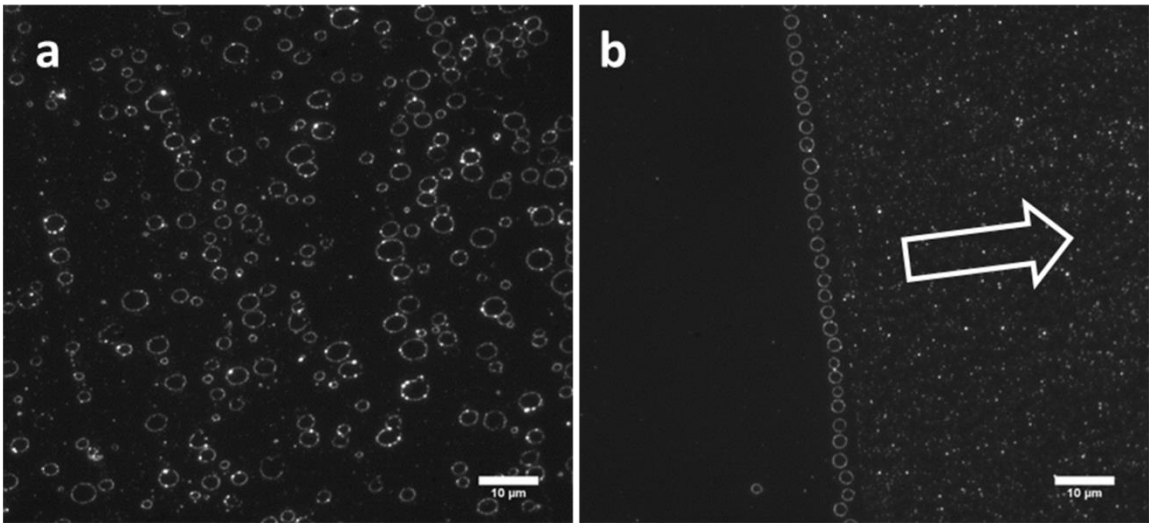

Figure 0.9. (a) QD rings deposited on a coverslip by dip-coating at an angle of ~ 35^{o}; (b) aligned QD rings by a controlled dip-coating method at an angle of ~ 45^{o}. The white arrow shows pulling direction of substrate in (b). Scale bars = 10 μm.

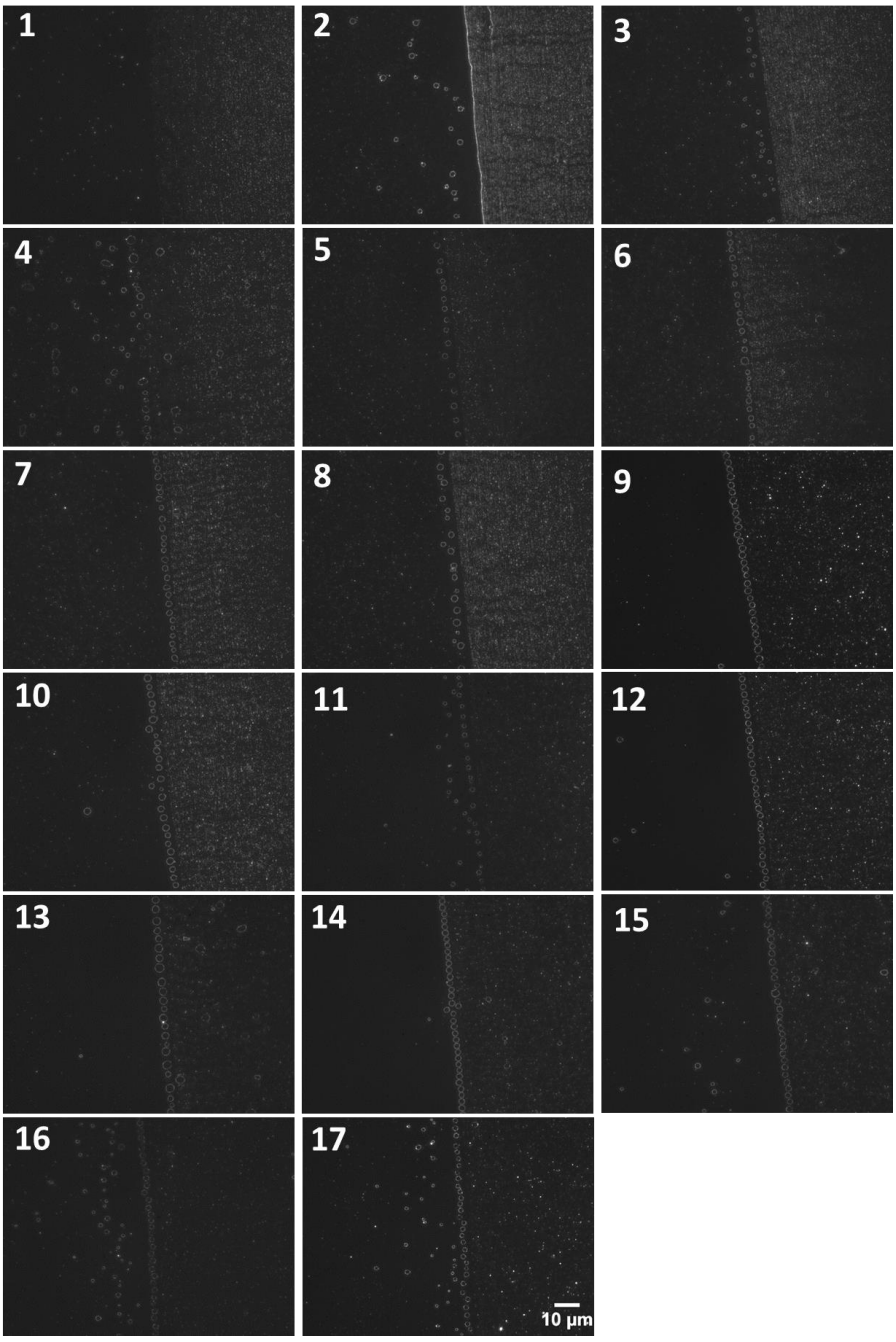

Figure 0.10. A series of images of aligned QD rings is shown with numbers indicating n-th pulling of the substrate. From the 5th pull, QD rings were consistently aligned along the contact line. Pulling direction of a substrate was towards right, and there exist aggregates of QDs deposited on the right side of QD ring alignments due to water evaporation during the stopping time.

3.4 Conclusion

We report 2-D self-assembly of PEG-functionalized QDs into rings at the air/water interface. This study emanated from the unanticipated observation of QD rings formed on the surface of droplets placed on coverslips. On clean (impurity-free) coverslips, surfactant were used to generate the QD rings. We manipulate the concentration of surfactant at the air/water interface to produce self-assembled surfactant islands (G-LE coexistence phase) driving QDs to adsorb at the 3-phase interface (air, water, and surfactant island) to reduce interfacial energy, thereby resulting in the formation of QD rings. The deposition and alignment of QD rings onto large area was demonstrated by dip-coating. The method demonstrated here for the fabrication of QD rings is very simple, and allows for a large area deposition by dip-coating without requiring complex template fabrication steps.

3.5 References

1. Chen, J., et al., *Evaporation-Induced Assembly of Quantum Dots into Nanorings.* ACS Nano, 2008. **3**(1): p. 173-180.

2. Kim, H.S., et al., *Nanoparticle Stripes, Grids, and Ribbons Produced by Flow Coating.* Advanced Materials, 2010. **22**(41): p. 4600-4604.

3. Tang, Z., N.A. Kotov, and M. Giersig, *Spontaneous Organization of Single CdTe Nanoparticles into Luminescent Nanowires.* Science, 2002. **297**(5579): p. 237-240.

4. Lu, N., et al., *Lateral Patterning of Luminescent CdSe Nanocrystals by Selective Dewetting from Self-Assembled Organic Templates.* Nano Letters, 2004. **4**(5): p. 885-888.

5. Henzie, J., et al., *Large-Area Nanoscale Patterning: Chemistry Meets Fabrication.* Accounts of Chemical Research, 2006. **39**(4): p. 249-257.

6. Anker, J.N., et al., *Biosensing with plasmonic nanosensors.* Nat Mater, 2008. **7**(6): p. 442-453.

7. Lee, D.Y., et al., *Macroscopic Nanoparticle Ribbons and Fabrics.* Advanced Materials, 2013. **25**(9): p. 1248-1253.

8. Keng, P.Y., et al., *Synthesis and Self-Assembly of Polymer-Coated Ferromagnetic Nanoparticles.* ACS Nano, 2007. **1**(4): p. 279-292.

9. Babayan, Y., et al., *Templated and Hierarchical Assembly of CdSe/ZnS Quantum Dots.* Advanced Materials, 2004. **16**(15): p. 1341-1345.

10. Gleiche, M., L.F. Chi, and H. Fuchs, *Nanoscopic channel lattices with controlled anisotropic wetting.* Nature, 2000. **403**(6766): p. 173-175.

11. Werts, M.H.V., et al., *Nanometer Scale Patterning of Langmuir−Blodgett Films of Gold Nanoparticles by Electron Beam Lithography.* Nano Letters, 2001. **2**(1): p. 43-47.

12. Ancona, M.G., et al., *Patterning of Narrow Au Nanocluster Lines Using V2O5 Nanowire Masks and Ion-Beam Milling.* Nano Letters, 2002. **3**(2): p. 135-138.

13. Pauzauskie, P.J., D.J. Sirbuly, and P. Yang, *Semiconductor Nanowire Ring Resonator Laser.* Physical Review Letters, 2006. **96**(14): p. 143903.

14. Lorke, A., et al., *Spectroscopy of Nanoscopic Semiconductor Rings.* Physical Review Letters, 2000. **84**(10): p. 2223-2226.

15. Bozhevolnyi, S.I., et al., *Channel plasmon subwavelength waveguide components including interferometers and ring resonators.* Nature, 2006. **440**(7083): p. 508-511.

16. Ramakrishna, G., et al., *Interparticle Electromagnetic Coupling in Assembled Gold-Necklace Nanoparticles.* Journal of the American Chemical Society, 2007. **129**(7): p. 1848-1849.

17. Kyung-Young, J., F.L. Teixeira, and R.M. Reano, *Au/SiO_2 Nanoring Plasmon Waveguides at Optical Communication Band.* Lightwave Technology, Journal of, 2007. **25**(9): p. 2757-2765.

18. Boker, A., et al., *Hierarchical nanoparticle assemblies formed by decorating breath figures.* Nat Mater, 2004. **3**(5): p. 302-306.

19. Khanal, B.P. and E.R. Zubarev, *Rings of Nanorods.* Angewandte Chemie, 2007. **119**(13): p. 2245-2248.

20. Sudeep, P.K., et al., *Monodisperse Oligo(phenylene vinylene) Ligands on CdSe Quantum Dots: Synthesis and Polarization Anisotropy Measurements.* Journal of the American Chemical Society, 2008. ***130***(8): p. 2384-2385.

21. Dabbousi, B.O., et al., *(CdSe)ZnS Core-Shell Quantum Dots: Synthesis and Characterization of a Size Series of Highly Luminescent Nanocrystallites.* The Journal of Physical Chemistry B, 1997. ***101***(46): p. 9463-9475.

22. Bae, W.K., et al., *Single-Step Synthesis of Quantum Dots with Chemical Composition Gradients.* Chemistry of Materials, 2008. **20**(2): p. 531-539.

23. Yu, W.W., et al., *Experimental Determination of the Extinction Coefficient of CdTe, CdSe, and CdS Nanocrystals.* Chemistry of Materials, 2003. ***15***(14): p. 2854-2860.

24. Uyeda, H.T., et al., *Synthesis of Compact Multidentate Ligands to Prepare Stable Hydrophilic Quantum Dot Fluorophores.* Journal of the American Chemical Society, 2005. **127**(11): p. 3870-3878.

25. Mei, B.C., et al., *Polyethylene glycol-based bidentate ligands to enhance quantum dot and gold nanoparticle stability in biological media.* Nat. Protocols, 2009. **4**(3): p. 412-423.

26. Sumner, A.L., et al., *The nature of water on surfaces of laboratory systems and implications for heterogeneous chemistry in the troposphere.* Physical Chemistry Chemical Physics, 2004. **6**(3): p. 604-613.

27. Zhu, J.-H., et al., *Acrylamide as cosurfactant and hydrotrope in the pseudoternary Span 80-Tween 85/isopar M/water emulsion/microemulsion forming system.* Colloids and Surfaces A: Physicochemical and Engineering Aspects, 2006. **290**(1–3): p. 19-24.

28. Aveyard, R., B.P. Binks, and J.H. Clint, *Emulsions stabilised solely by colloidal particles.* Advances in Colloid and Interface Science, 2003. **100–102**(0): p. 503-546.

29. Honig, D., G.A. Overbeck, and D. Mobius, *Morphology of pentadecanoic acid monolayers at the air/water interface studied by BAM.* Advanced Materials, 1992. **4**(6): p. 419-424.

30. Moore, B.G., et al., *Phase diagram of Langmuir monolayers of pentadecanoic acid: quantitative comparison of surface pressure and fluorescence microscopy results.* The Journal of Physical Chemistry, 1990. **94**(11): p. 4588-4595.

31. Henon, S. and J. Meunier, *Microscope at the Brewster angle: Direct observation of first-order phase transitions in monolayers.* Review of Scientific Instruments, 1991. **62**(4): p. 936-939.

32. Kaganer, V.M., H. Möhwald, and P. Dutta, *Structure and phase transitions in Langmuir monolayers.* Reviews of Modern Physics, 1999. **71**(3): p. 779-819.

CHAPTER 4

FLOW DYNAMICS WITHIN AN EVAPORATING DROPLET

4.1 Introduction

Evaporation of solutions has been widely proposed and demonstrated as a way to assemble solutes (e.g. polymers, DNA, microspheres, nanoparticles) into ordered structures on substrates.[1-8] This assembly from suspended solutes is dependent on evaporation-induced flow dynamics, which are generally associated with the phenomenon commonly called the "coffee ring effect". This effect, first explained by Deegan and co-workers, refers to the non-uniform deposition of solutes near the contact line due to mass transport balance when the contact line of the evaporating coffee droplet is pinned.[9] Since evaporation flux is greater at the edge of the droplet compared to the top, a flow is generated from the center toward the edge to compensate for solvent mass loss.[10] The characteristics of this flow are dependent on several factors, including the evaporation rate, evaporation flux distribution over the droplet surface, and the contact angle.

There have been several theoretical and analytical studies of this important mass transport phenomenon. Deegan and co-workers derived the height averaged radial velocity and successfully predicted the time-dependent radial distribution of solute particles.[9, 11] Hu and Larson developed an expression to map the locally resolved axisymmetric flow field in a slowly evaporating droplet with a pinned contact line using analytical and finite element analysis (FEA), both with and without a Marangoni flow effect.[12, 13] Petsi and Burganos

also considered this problem and provided an analytical solution for any contact angle of an infinitely long cylindrical liquid evaporating on hydrophilic and hydrophobic substrates.[14] For continued development of evaporative assembly as a scalable process, it is particularly important to understand the effect of contact angle on radial velocity. The relationship between the contact angle and the radial velocity is important because as contact angle decreases with time during evaporation, the evaporation flux at the edge increases despite the total evaporation flux remaining approximately the same.[10] This increase in the evaporation flux at the edge generates a faster flow, hence faster solute assembly. Although there has been considerable theoretical work on the flow dynamics within evaporating droplets, to our knowledge there has been limited, if any, experimental verification of these derived relationships. A better experimental understanding of this effect will improve the time efficiency of these processes and quality of the assembly.

In this chapter, we present the experimental measurement of height averaged radial velocity in the range of contact angles, 5-50^{o}, and at different evaporation rates using a particle tracking method, and compare the results with a previous theoretical study by Hu and Larson. We find good agreement between theory and experiment, and we develop a simplified equation to relate the height averaged radial velocity to evaporation rate (k) and the contact angle (θ). This simple relationship provides clear design rules that are expected to guide the scaling up of process speeds and scaling down of structural dimensions for evaporative assembly methods.

4.2 Experimental

4.2.1 Octadecyltrichlorosilane (OTS) Coating on Coverslips.

A coverslip (VWR micro cover glass No. 1.5) was sonicated in toluene for 20 min and subjected to UV/ozone treatment for 30 min. The cleaned coverslip was immersed in 0.1 v/v% OTS in toluene, and the solution was stirred for 1 h. The OTS treated coverslip was then washed with toluene and isopropanol several times. The water contact angle of the OTS treated coverslip was measured as ~90-100^{o}. To control the water contact angle of the OTS treated substrates, the substrates were exposed to UV/ozone to partially oxidize the OTS layer. For a ~6 min UV/ozone exposure time, the water contact angle of the OTS treated coverslip was reduced to ~35^{o}.

4.2.2 Particle Tracking

1 μL of a water droplet containing 1 μm latex particles (0.00004 vol%) was placed on an OTS-treated coverslip on an inverted fluorescence microscope (Zeiss Axiovert 200) equipped with a CCD camera (Retiga 2000R), and another CCD camera (Pixelink) was utilized for viewing the side view of droplets to measure contact angle change with time. Fluorescent particles suspended in a droplet were recorded in gray scale every 120 ms, and the side view images of the droplet were taken every 12 s. 100 Successive fluorescent particle images were stacked to generate an image with overlapped particle images, and the first and last image of each stack are processed to afford green and red color, respectively. In this way, each 100-image stack has continuous trajectories starting from green to red dots indicating the direction of particle motion. The distance from the green to red particles was measured using ImageJ software to obtain individual radial velocity.

4.3 Results and Discussion

4.3.1 Effect of Contact Angle on Radial Flow Dynamics

The radial flow dynamics were observed by tracking the motion of individual 1 μm fluorescent colloid particles within an evaporating water droplet. We tracked particles in three different radial positions, $\mathbb{r} = r/R$ (A = 1-0.8, B = 0.8-0.65, and C = 0.65-0.5) where R is the radius of a droplet, and r is radial distance from the center depicted in Figure 4.1a, during the evaporation. To create a single overlapped particle images, 100 successive fluorescent particle images were stacked, where the first and last frame of each stack were processed to afford green and red in color, respectively. In this way, each stack has continuous trajectories starting from green to red dots indicating the direction of particle motions. A representative stack of images is shown in Figure 4.1b.

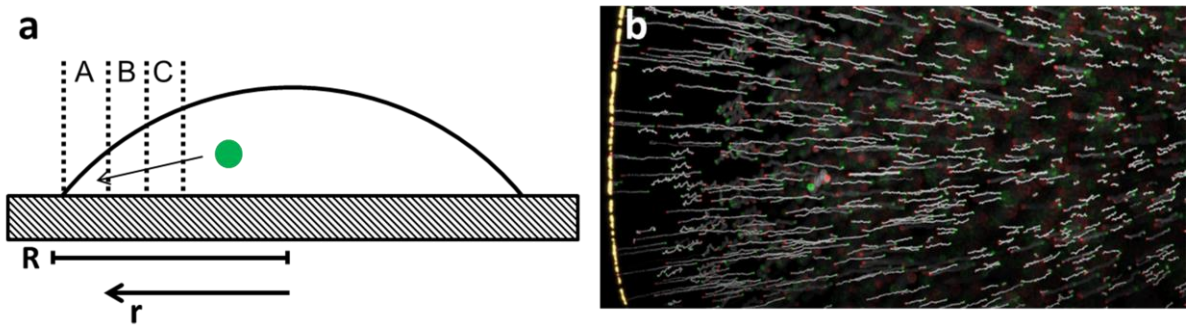

Figure 0.1. (a) A stacked series of images after image processing shows a number of particle trajectories moving from the center to the contact line (green to red dots). (b) A schematic of a droplet with different radial positions (A, B, C) with a green dot moving towards the edge due to the capillary flow while the contact line is pinned.

These stacked images were used to measure the radial flow velocity as a function of contact angle θ. The distances of all particle trajectories from each stack were measured, and divided by time interval (12 s) for different radial positions, providing the measurement of height averaged radial velocities since all particles at different heights within a depth of focus are considered. Also, we tracked particles at different focal planes which allows for the comparison between the height averaged radial velocities determined at different focal planes. The range of contact angles, θ, in this experiment was ~5-50^{o} using two OTS treated substrates with different extent of oxidation as described in the Experimental section. During evaporation, the droplets on the substrate with a high initial contact angle (~50 ^{o}) began receding when the contact angle reached ~20^{o}, and droplets on the substrate with a low initial contact angle (~35 ^{o}) remained pinned until the contact angle ~5-10^{o}.

In Figure 4.2a are shown plots of the height averaged radial velocities at different focal planes as a function of contact angle, θ. In general, the radial velocity increases with decreasing θ. This is due to mass conservation; the water flows faster radially within a thinner droplet to replenish the water loss by evaporation at the edge as the evaporation rate remains the same throughout the experiments.[10] The data in Figure 4.2a also shows that the height averaged radial velocities at different focal planes fall onto a single curve. Although radial velocity seems independent of height within a given range of focal planes examined in this experiment, this apparent independence is due to large depth of focus (DOF), which is approximately 100 μm, for our measurement system. Furthermore, only projected distances were considered, however in reality, the particles have 3-D displacements. Also, even particles out of DOF are carried into the DOF shortly due to the decrease in contact angle θ with time. Figure 4.2b shows the height averaged radial velocity as a function of θ for three

radial positions. For each radial position, the radial velocity increases with decreasing θ, seemingly following a similar power law trend for all three regions (A, B, and C). Furthermore, the magnitude of the radial velocity at a given θ is found to increase with increasing radial position, ℟ = r/R.

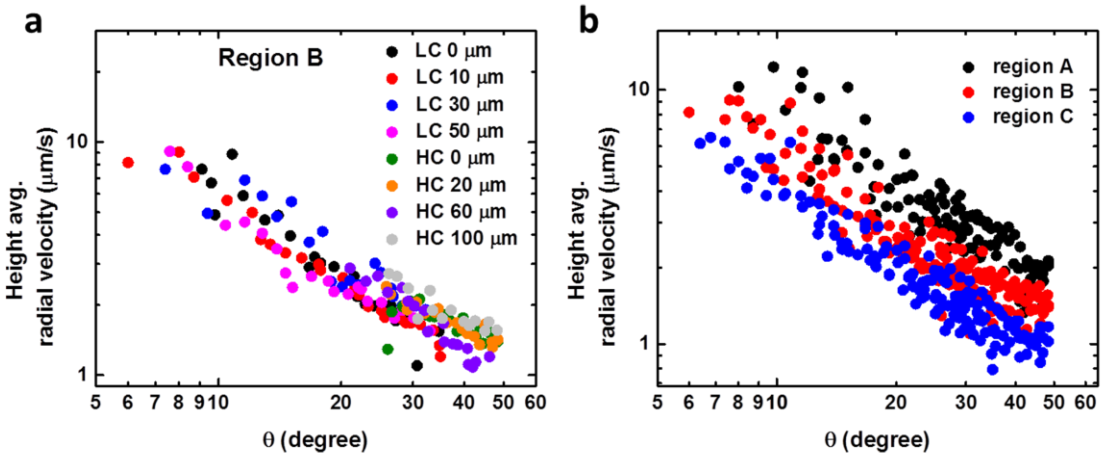

Figure 0.2. (a) The log-log plot of height averaged radial velocity at radial position B (r/R = 0.65-0.8) with contact angle for different focal planes from the surface of the substrate. In the legend, LC and HC refer to low and high contact angle, respectively, for two different substrates used in this experiment and the focal plane height is indicated in μm. Plot (a) is the same as the plot in (b) for region B (red dots). (b) A log-log plot of height averaged radial velocity at three different radial positions with regard to contact angles.

4.3.2 Effect of Evaporation Rate on Radial Flow Dynamics

In addition to the magnitude increasing with radial positions, the magnitude of the radial velocity is directly related to the evaporation rate. To demonstrate this, the humidity was increased to slow the evaporation rate of a droplet. Figures 4.3(a and b) show the droplet

volume, V, and as θ a function of time for both humidity levels, respectively. The magnitude of the slopes, k = |dθ/dt|, in Figure 4.3b are related to the evaporation rate, dV/dt, in Figure 4.3a according to the correlation between volume V and θ [10] : $\frac{dV}{d\theta} = \frac{\pi R^3}{4}\left(1 + \frac{\theta^2}{4}\right)$ is derived from $V = \frac{\pi}{6} R^3 \tan\frac{\theta}{2}\left[3 + \left(\tan\frac{\theta}{2}\right)^2\right]$ using small angle approximation of tangent function ($\tan\theta \approx \theta$ with less than 5% error within $0 \leq \theta \leq 0.7$ in radian) such that $dV/dt = (dV/d\theta)(-k)$. Since $dV/d\theta$ is almost a constant at a given range of θ as shown in Figure 4.3c, k is proportional to the evaporation rate in a given condition, $0 \leq \theta \leq 0.7$ in radian comparable to $0 \leq \theta \leq \sim 40^o$ (k = 0.03 deg/sec for the slow evaporation and k = 0.1 deg/sec for the ambient condition).

Figure 4.3d shows the height averaged radial velocity as a function of θ for both evaporation rates. For both rates, the radial velocity increases with decreasing θ, and the relative velocity at a fixed θ is greater for the higher evaporation rate. The faster the rate of water loss at the edge is, the faster the capillary flow is. Interestingly, for a slowly evaporating droplet, there exists a range of $20^o < \theta < 40^o$, where the radial velocity plateaus. This velocity independence is likely due to the capillary flow weakening at high θ and a slow evaporation rates, resulting in the Brownian motion of colloid beads dominating over capillary flow.

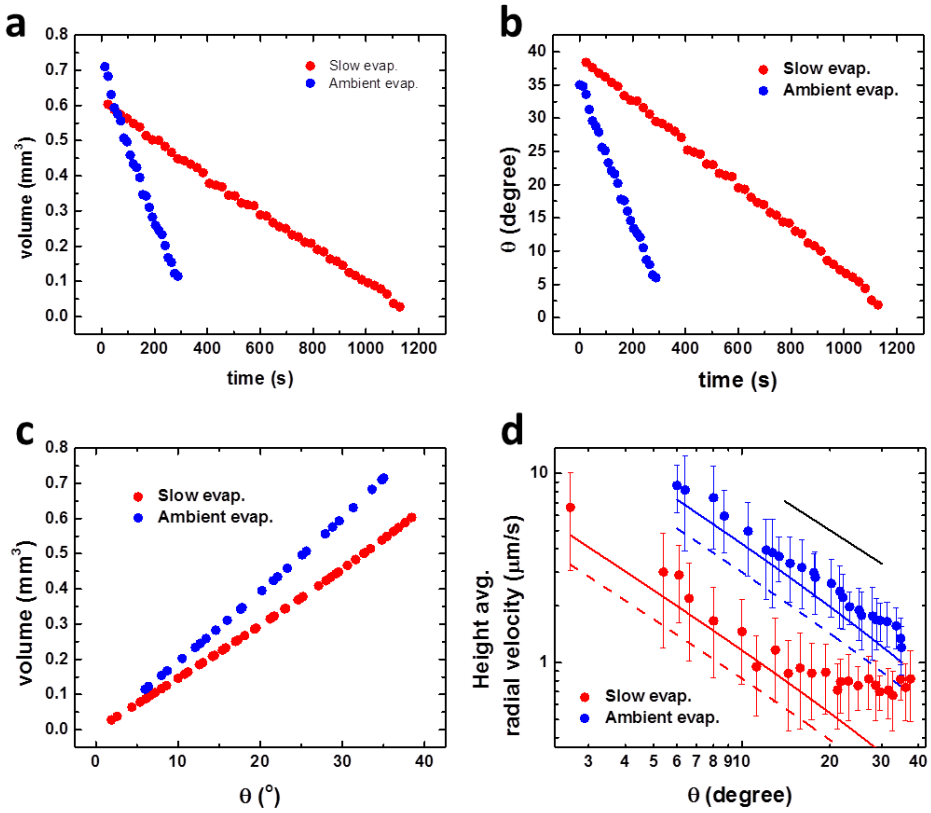

Figure 0.3. (a) Plots of droplet volume as a function of time for slow and ambient evaporation rates. (b) Plots of contact angle as a function of contact angle θ, which gives a linear trend. (c) Plots of droplet volume as a function of contact angle θ. (d) The log-log plots (solid circle) of height averaged radial velocity with regard to contact angle at radial position B for slow and ambient evaporation environments. Solid and dotted lines are drawn based on the equation (2) for height averaged radial velocity with two different radial positions, r/R = 0.8 for solid lines and 0.65 for dotted lines. The black solid line is for the exponent value -1 of a power law.

4.3.3 Comparison of Experimental Results to Analytical Prediction

Thus far, we experimentally presented the height averaged radial velocity profile with regard to both θ and k, where radial flow velocity increases with decreasing θ and increasing

k. These experimental results were compared with the analytical predictions developed by Hu and Larson as shown below.[13]

$$\mathbb{u} = 0.25\frac{R}{t_f - t(\theta)}\frac{1}{\mathbb{r}}\left[(1-\mathbb{r}^2)^{-\lambda(\theta)} - (1-\mathbb{r}^2)\right] \qquad (1)$$

where $\mathbb{u}$ is height averaged radial velocity, $\mathbb{r}$ = r/R, t(θ) is the experimental time at θ, t_f is the total evaporation time, and $\lambda(\theta) = 0.5 - \frac{\theta}{180}$ indicating the uniformity of evaporation across the surface, which is empirically determined by using a FEA.[10] The evaporation flux along the droplet surface is uniform at θ = 90° (λ = 0) and becomes non-uniform towards θ = 0° (λ = 0.5). The term, t_f - t(θ),can be rewritten as a function of θ/k since t(θ) = -θ/k + t_f as found in Figure 4.3b. Thus, equation (1) can be rewritten as.

$$\mathbb{u} = 0.25\frac{Rk}{\theta}\frac{1}{\mathbb{r}}\left[(1-\mathbb{r}^2)^{-\lambda(\theta)} - (1-\mathbb{r}^2)\right] \qquad (2)$$

Equation (2) contains information on both θ and k and was plotted (dotted and solid line) as a function of θ with known values of R, k, and $\mathbb{r}$ to be compared with our experimental plots (solid circles) in Figure 4.3d. Since the experimental values of height averaged radial velocities are measured within a certain range of radial position such as $\mathbb{r}$ = 0.65-0.8, an analytical equation was plotted with two different radial positions, $\mathbb{r}$ = 0.65 and 0.8 for dotted and solid line, respectively. As shown in Figure 4.3d, experimental results are in a good agreement with analytical predictions within experimental errors.

4.3.4 Modification of Analytical Equation

We found that the trend is close to a power law, which is a much more insightful form than equation (1), due to small contribution of the last term, S, to the θ dependence, S = $\frac{1}{\mathbb{r}}\left[(1-\mathbb{r}^2)^{-\lambda(\theta)}-(1-\mathbb{r}^2)\right]$. Thus, we were determined to modify the equation (2) to a simpler form such that it can provide the impact of θ on $\mathbb{u}$ as a scaling. It is empirically found that S can be described well by an exponential fit to give $\mathbb{u} = 0.25\frac{Rk}{\theta}\left[A\ exp\left(\frac{-\theta}{\tau}\right)\right]$ (Figure 4.4a). Then, this can be approximated using Taylor's series to give,

$$\mathbb{u} = 0.25\ \mathrm{A\ R\ k}\left[\frac{1}{\theta}-\frac{1}{\tau(\mathbb{r})}\right] \qquad (3)$$

$$\mathbb{u} \sim \frac{k}{\theta} \qquad (4)$$

Therefore, $\mathbb{u}$ is proportional to k and inversely proportional to θ as a simple scaling equation (4). Accordingly, this simple power law θ^{-1} is drawn into Figure 4.3d as a solid black line showing a good prediction of the trend of radial flow velocities as a function of θ for the radial position B. This scaling prediction is also valid for positions close to the contact line since the slope does not change with positions as shown in Figure 4.2b, only shifting vertically as function of radial positions. However, we note that the exact value of velocity calculated from equation (3) will have increasing error as r/R approaches 1 due to poor approximation with larger θ/τ where τ is a function of r/R.

This simple power law relationship is most important in the design of evaporative assembly, where suspended solutes move at different speed towards the contact line.

Evaporative assembly has many attractive attributes over complexity, cost, scale, and throughput, however the required processing times to achieve high fidelity continuous structures has been a drawback. As presented, the scaling equation (4) isolates two key parameters, k and θ, to maximize assembly rate and uniformity. For high assembly rates, k must be large and θ must be small. For uniformity, it is critical that θ is constant across relevant lateral length scales. Both of these lessons were critical in the development of a recent evaporative assembly method, called flexible blade flow coating.[7] In this method, a dilute solution of particles in an organic solvent is trapped by capillary forces between a flexible blade and a rigid substrate. The flexibility of the blades allows θ to be uniform across the full width of macroscopic blades, while the organic solvent allows k to be large. With this method, assemblies of CdSe nanoparticles were created with dimensions of width ~250 nm, height ~10 nm, and length ~ 10 cm.[7] This simplified estimation of radial flow velocity will help understand and manipulate the evaporative assembly processes on different substrates (different θ) in terms of both required experimental time for assembly and structural dimensions, such as width and/or height of assembled structures. [6-8]

4.3.4 Approximation Error

$$\mathbb{u} = 0.25\frac{Rk}{\theta}\left[A\ exp\left(\frac{-\theta}{\tau}\right)\right] \qquad (5)$$

$$\mathbb{u} = 0.25\ \mathrm{A\ R\ k}\left[\frac{1}{\theta} - \frac{1}{\tau(\mathbb{r})} + \frac{\theta}{2\tau(\mathbb{r})^2}\right] \qquad (6)$$

$$\mathbb{u} = 0.25\ \mathrm{A\ R\ k}\left[\frac{1}{\theta} - \frac{1}{\tau(\mathbb{r})}\right] \qquad (3)$$

Equation (6) is approximated from equation (5) by Taylor's series up to the third term, and equation (3) is approximated up to second term since the value of θ/τ is smaller than unity. However, as θ/τ approaches unity, the approximation has increasing error for the exact value of height averaged radial velocity. Thus, we qualitatively examined the approximation in the range of $\mathbb{r} = \mathrm{r/R}$ up to 0.999. In Figure 4.5a is shown the variability of θ/τ as function of τ in the range of $21 < \tau < 200$ for four contact angles, 5, 10, 12, 20 and 30^o. The range of τ is determined from the range of $0.5 < \mathbb{r} < 0.999$ in Figure 4.4b. Figure 4.5b shows the error of this approximation as a function of θ/τ for approximations with two terms and three terms of Taylor series. If the contact angle is around 5^o, the approximation could be reduced with two terms with error less than ~ 2% at any radial position, $\mathbb{r}$. However, the error increases rapidly up to ~ 18% with the contact angle of 10^o at $\mathbb{r} = 0.999$, where the approximation with equation (3) seems not reasonable, as opposed to ~ 3% error with equation (6). At radial position $\mathbb{r} = 0.97$ which is very close to contact line, equation (3) can be applied to contact angles up to ~ 12^o with error less than ~ 2%, which is most cases of flow coating conditions using organic solvents. For higher contact angles, equation (6) can be applied with an error less than ~ 3%. Generally, the exact value of velocity calculated from equation (6) and (3) has an error increasing with increasing θ and increasing $\mathbb{r}$, in which case θ/τ increases. However, the power law scaling prediction is valid for any positions close to the contact line since the slope does not change with positions, only shifting vertically as function of radial position and evaporation rate.

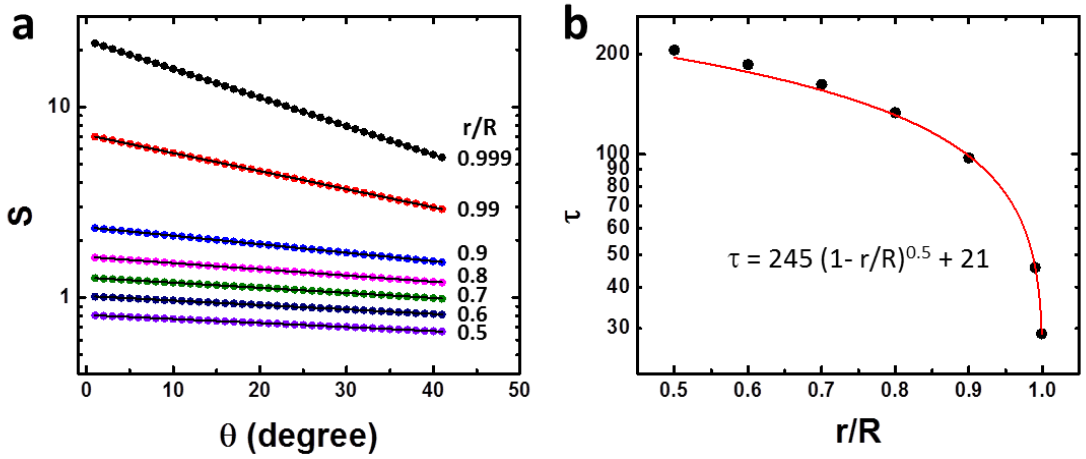

Figure 0.4. (a) Plots of S (solid circles) as a function of θ for different radial positions, $\mathbb{r}$ = r/R are fitted by an exponential function, A·exp(-θ/τ) (black solid lines). (b) Plot of τ as a function of r/R up to 0.999 is best described by an equation, $\tau = 245\ (1-\mathbb{r})^{0.5} + 21$.

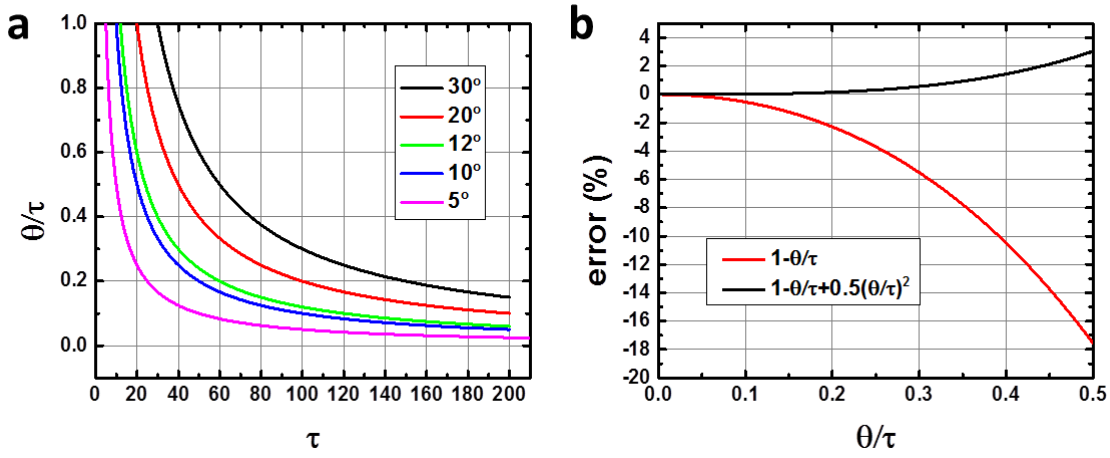

Figure 0.5. (a) The plot of the value of θ/τ as a function of t for different contact angles, 5, 10, 12, 20, and 30°. (b) The plot of errors as a function of the value of θ/τ for equation (6) and (3).

4.4 Conclusion

We have demonstrated experimentally that the magnitude of capillary flow during evaporation of a pinned droplet is non-linearly dependent on the contact angle. The flow velocity increases as the contact angle decreases for contact angle ranging from almost 5 - 50^{o}. This resulting trend can be quantitatively described by modifying Hu and Larson's analytical equation. The simplified estimation demonstrates that θ and k are primary parameters in evaporative assembly processes. This study allows us to understand the effect of substrate surface property on assembled structures and kinetics in evaporative assembly processes, such as flow coating.

4.5 References

1. Jing, J., et al., *Automated high resolution optical mapping using arrayed, fluid-fixed DNA molecules.* Proceedings of the National Academy of Sciences, 1998. **95**(14): p. 8046-8051.

2. Deegan, R.D., *Pattern formation in drying drops.* Physical Review E, 2000. **61**(1): p. 475-485.

3. Senses, E., et al., *Spatial Ordering of Colloids in a Drying Aqueous Polymer Droplet.* Langmuir, 2013. **29**(8): p. 2588-2594.

4. Yunker, P.J., et al., *Suppression of the coffee-ring effect by shape-dependent capillary interactions.* Nature, 2011. **476**(7360): p. 308-311.

5. Truskett, V.N. and K.J. Stebe, *Influence of Surfactants on an Evaporating Drop: Fluorescence Images and Particle Deposition Patterns.* Langmuir, 2003. **19**(20): p. 8271-8279.

6. Kim, H.S., et al., *Nanoparticle Stripes, Grids, and Ribbons Produced by Flow Coating.* Advanced Materials, 2010. **22**(41): p. 4600-4604.

7. Lee, D.Y., et al., *Macroscopic Nanoparticle Ribbons and Fabrics.* Advanced Materials, 2013. **25**(9): p. 1248-1253.

8. Pham, J.T., et al., *Highly Stretchable Nanoparticle Helices Through Geometric Asymmetry and Surface Forces.* Advanced Materials, 2013: p. 1-6.

9. Deegan, R.D., et al., *Capillary flow as the cause of ring stains from dried liquid drops.* Nature, 1997. **389**(6653): p. 827-829.

10. Hu, H. and R.G. Larson, *Evaporation of a Sessile Droplet on a Substrate.* The Journal of Physical Chemistry B, 2002. **106**(6): p. 1334-1344.

11. Deegan, R.D., et al., *Contact line deposits in an evaporating drop.* Physical Review E, 2000. **62**(1): p. 756-765.

12. Hu, H. and R.G. Larson, *Analysis of the Effects of Marangoni Stresses on the Microflow in an Evaporating Sessile Droplet.* Langmuir, 2005. **21**(9): p. 3972-3980.

13. Hu, H. and R.G. Larson, *Analysis of the Microfluid Flow in an Evaporating Sessile Droplet.* Langmuir, 2005. **21**(9): p. 3963-3971.

14. Petsi, A.J. and V.N. Burganos, *Evaporation-induced flow in an inviscid liquid line at any contact angle.* Physical Review E, 2006. **73**(4): p. 041201.

CHAPTER 5

CONCLUSION

The focus of this thesis is the use of fluorescent particles as a probe to reveal anomalous dynamics and assembly processes occurring within materials of interest, i.e., polymer gels and aqueous solution. In Chapter 2, we used CdSe/ZnS Core/Shell QDs covered with carboxylate ligands as a fluorescent probe within structurally complex PAAm hydrogels to discover the anomalous diffusion of QDs and structural heterogeneities of polyacrylamide hydrogels with increasing cross-linker content by tracking single QDs. The surface chemistry with hydrophilic ligand, carboxylate, rendering the QDs water-soluble, photo-stable, and highly fluorescent in aqueous solution made it possible for accurately tracking individual single QDs, which has been the largest obstacles to researchers. By adopting the formalism of continuous time random walk (CTRW) with a specific model, the random trap (RT) model, we studied the transient caging times extracted from experimental data to obtain the information about the energetic landscape of gel networks which suggests the extent of structural heterogeneity of PAAm hydrogels. This is, to our knowledge, the first successful experimental demonstration of single particle tracking using QDs within synthetic polymer hydrogels, where the small size of QDs, which is larger than dye molecules, affords diffusing motion that can explore the complex structures of gel networks. If extended to multi-color imaging of several different QD probe sizes, we anticipate that this experimental method has the potential to provide a wealth of information on the structures of a wide variety of networks with nanometer-scale porosities, and should yield sensitive tests of more refined models for the landscape of trap energies within these materials.

In Chapter 3, we studied the formation of QD (CdSe/ZnS Core/Shell QD covered with PEG ligands) rings at the air/water interface by "2-D Pickering emulsions". Dispersed QDs in bulk phase (water) allowed the assembly of surfactant islands visualized at the air/water interface by being absorbed onto the interfacial line. The formation of QD rings discovered at the interface introduces a simple method for nanoparticle assemblies without the need of templates or costly ion-beam etching processes. Since this assembly of QD rings occur only at the interface, they were easily transferred to other substrates by dip coating. Furthermore, patterning of QD rings were successfully demonstrated on other substrate by controlled dip coating. These patterned and deposited QD rings have a potential to be applied for optical and electronic resonators. The key to a better and consistent assembly of QD rings by this method is the kinetics of each component participating in this assembly system. Surfactants should first form islands at the air/water interface, then, followed by the adsorption of QDs into interfacial lines of islands. That is, if QDs are absorbed to the interface before surfactant islands are formed, no QD rings can be assembled. Therefore, fine control over the introduction of surfactants or QDs into the system would greatly enhance the robustness of this method for the interfacial assembly of nanoparticles.

Lastly, in Chapter 4, suspended fluorescent latex beads were used to quantify the radial flow generated within an evaporating droplet due to the phenomenon commonly called the "coffee ring effect". With controlled contact angle of glass surfaces, we studied the effect of contact angle on the radial flow dynamics by tracking individual probe particles drifting within droplets. Our experimental results agreed well with the analytical prediction by Hu and Larson, which is, to our knowledge, the first empirical verification of the previous theoretical

studies. Additionally, we found that the original equation can be reduced to a simple power law as a function of contact angle and evaporation rate. This study could help understand the effect of substrates on the kinetics or efficiency of evaporative assembly of ordered structures constructed by e.g., flexible blade flow coating. For future work, the dimensions of ordered structures constructed by flow coating as a function of hydrophobicity of substrates should be examined by applying this simple power law to predict the kinetics of assembly.

BIBLIOGRAPHY

Ancona, M. G., S. E. Kooi, et al. (2002). "Patterning of Narrow Au Nanocluster Lines Using V_2O_5 Nanowire Masks and Ion-Beam Milling." Nano Letters **3**(2): 135-138.

Anker, J. N., W. P. Hall, et al. (2008). "Biosensing with plasmonic nanosensors." Nat Mater **7**(6): 442-453.

Annaka, M., T. Matsuura, et al. (2003). "Preparation of Comb-Type N-Isopropylacrylamide Hydrogel Beads and Their Application for Size-Selective Separation Media." Biomacromolecules ***4***(2): 395-403.

Aveyard, R., B. P. Binks, et al. (2003). "Emulsions stabilised solely by colloidal particles." Advances in Colloid and Interface Science **100–102**(0): 503-546.

Babayan, Y., J. E. Barton, et al. (2004). "Templated and Hierarchical Assembly of CdSe/ZnS Quantum Dots." Advanced Materials **16**(15): 1341-1345.

Bae, W. K., K. Char, et al. (2008). "Single-Step Synthesis of Quantum Dots with Chemical Composition Gradients." Chemistry of Materials **20**(2): 531-539.

Bansil, R. and M. K. Gupta (1980). "EFFECT OF VARYING CROSSLINKING DENSITY ON POLYACRYLAMIDE GELS." Ferroelectrics ***30***(1-4): 63-71.

Barkai, E., Y. Garini, et al. (2012). "Strange kinetics of single molecules in living cells." Physics Today **65**(8): 29-35.

Bässler, H. (1981). "Localized states and electronic transport in single component organic solids with diagonal disorder." physica status solidi (b) **107**(1): 9-54.

Bastide, J. and L. Leibler (1988). "Large-scale heterogeneities in randomly cross-linked networks." Macromolecules ***21***(8): 2647-2649.

Berlin, Y. A., L. D. A. Siebbeles, et al. (1997). "Thermally activated diffusion along one-dimensional chains with energetic disorder: analysis of computer simulation data." Chemical Physics Letters **276**(5–6): 361-370.

Boker, A., Y. Lin, et al. (2004). "Hierarchical nanoparticle assemblies formed by decorating breath figures." Nat Mater **3**(5): 302-306.

Bouchaud, J.-P. and A. Georges (1990). "Anomalous diffusion in disordered media: Statistical mechanisms, models and physical applications." Physics Reports **195**(4–5): 127-293.

Bozhevolnyi, S. I., V. S. Volkov, et al. (2006). "Channel plasmon subwavelength waveguide components including interferometers and ring resonators." Nature **440**(7083): 508-511.

Burov, S. and E. Barkai (2011). "Time Transformation for Random Walks in the Quenched Trap Model." Physical Review Letters **106**(14): 140602.

Calvet, D., J. Y. Wong, et al. (2004). "Rheological Monitoring of Polyacrylamide Gelation: Importance of Cross-Link Density and Temperature." Macromolecules **37**(20): 7762-7771.

Chaudhuri, P., L. Berthier, et al. (2007). "Universal Nature of Particle Displacements close to Glass and Jamming Transitions." Physical Review Letters **99**(6): 060604.

Chaudhuri, P., Y. X. Gao, et al. (2008). "A random walk description of the heterogeneous glassy dynamics of attracting colloids." Journal of Physics-Condensed Matter **20**(24): 244126.

Chen, J., W.-S. Liao, et al. (2008). "Evaporation-Induced Assembly of Quantum Dots into Nanorings." ACS Nano **3**(1): 173-180.

Cheng, N.-S. (2008). "Formula for the Viscosity of a Glycerol−Water Mixture." Industrial & Engineering Chemistry Research **47**(9): 3285-3288.

Chrambach, A. and D. Rodbard (1971). "Polyacrylamide Gel Electrophoresis." Science ***172***(3982): 440-451.

Crocker, J. C. and D. G. Grier (1996). "Methods of Digital Video Microscopy for Colloidal Studies." Journal of Colloid and Interface Science **179**(1): 298-310.

Dabbousi, B. O., J. Rodriguez-Viejo, et al. (1997). "(CdSe)ZnS Core-Shell Quantum Dots: Synthesis and Characterization of a Size Series of Highly Luminescent Nanocrystallites." The Journal of Physical Chemistry B ***101***(46): 9463-9475.

Dahan, M., S. Levi, et al. (2003). "Diffusion Dynamics of Glycine Receptors Revealed by Single-Quantum Dot Tracking." Science **302**(5644): 442-445.

Dasgupta, B. R. and D. A. Weitz (2005). "Microrheology of cross-linked polyacrylamide networks." Physical Review E **71**(2): 021504.

Deegan, R. D. (2000). "Pattern formation in drying drops." Physical Review E **61**(1): 475-485.

Deegan, R. D., O. Bakajin, et al. (1997). "Capillary flow as the cause of ring stains from dried liquid drops." Nature **389**(6653): 827-829.

Deegan, R. D., O. Bakajin, et al. (2000). "Contact line deposits in an evaporating drop." Physical Review E **62**(1): 756-765.

Dickson, R. M., D. J. Norris, et al. (1996). "Three-Dimensional Imaging of Single Molecules Solvated in Pores of Poly(acrylamide) Gels." Science **274**(5289): 966-968.

Drazer, G., M. Rosen, et al. (2000). "Anomalous transport in activated carbon porous samples: power-law trapping-time distributions." Physica A: Statistical Mechanics and its Applications **283**(1–2): 181-186.

Drury, J. L. and D. J. Mooney (2003). "Hydrogels for tissue engineering: scaffold design variables and applications." Biomaterials ***24***(24): 4337-4351.

Elliott, L. C. C., M. Barhoum, et al. "Trajectory analysis of single molecules exhibiting non-Brownian motion." Physical Chemistry Chemical Physics **13**(10): 4326-4334.

Fawcett, J. S. and C. J. O. R. Morris (1966). "Molecular-sieve chromatography of proteins on granulated polyacrylamide gels." Separation science ***1***: 9-26.

Frauenfelder, H., S. Sligar, et al. (1991). "The energy landscapes and motions of proteins." Science **254**(5038): 1598-1603.

Fu, Y., F. Ye, et al. (2006). "Single Molecule Spectroscopy Studies of Diffusion in Mesoporous Silica Thin Films." The Journal of Physical Chemistry B **110**(18): 9164-9170.

Gao, Y. and M. L. Kilfoil (2009). "Intermittent and spatially heterogeneous single-particle dynamics close to colloidal gelation." Physical Review E **79**(5): 051406.

Gleiche, M., L. F. Chi, et al. (2000). "Nanoscopic channel lattices with controlled anisotropic wetting." Nature **403**(6766): 173-175.

Haramagatti, C. R., F. H. Schacher, et al. "Diblock copolymer membranes investigated by single-particle tracking." Physical Chemistry Chemical Physics **13**(6): 2278-2284.

Haus, J. W. and K. W. Kehr (1987). "Diffusion in regular and disordered lattices." Physics Reports **150**(5–6): 263-406.

Havlin, S. and D. Ben-Avraham (2002). "Diffusion in disordered media." Advances in Physics **51**(1): 187-292.

He, K., F. Babaye Khorasani, et al. (2013). "Diffusive Dynamics of Nanoparticles in Arrays of Nanoposts." ACS Nano **7**(6): 5122-5130.

Hecht, A. M., R. Duplessix, et al. (1985). "Structural inhomogeneities in the range 2.5-2500 Å in polyacrylamide gels." Macromolecules ***18***(11): 2167-2173.

Heitjans, P. and J. Karger, Eds. (2005). Diffusion in condensed matter.

Henon, S. and J. Meunier (1991). "Microscope at the Brewster angle: Direct observation of first-order phase transitions in monolayers." Review of Scientific Instruments **62**(4): 936-939.

Henzie, J., J. E. Barton, et al. (2006). "Large-Area Nanoscale Patterning: Chemistry Meets Fabrication." Accounts of Chemical Research **39**(4): 249-257.

Hoare, T. R. and D. S. Kohane (2008). "Hydrogels in drug delivery: Progress and challenges." Polymer ***49***(8): 1993-2007.

Holmes, D. L. and N. C. Stellwagen (1991). "Estimation of polyacrylamide gel pore size from Ferguson plots of linear DNA fragments. II. Comparison of gels with different crosslinker concentrations, added agarose and added linear polyacrylamide." ELECTROPHORESIS **12**(9): 612-619.

Holtzer, L., T. Meckel, et al. (2007). "Nanometric three-dimensional tracking of individual quantum dots in cells." Applied Physics Letters **90**(5): 053902-053903.

Honig, D., G. A. Overbeck, et al. (1992). "Morphology of pentadecanoic acid monolayers at the air/water interface studied by BAM." Advanced Materials **4**(6): 419-424.

Hsu, T. P. and C. Cohen (1984). "Observations on the Structure of a Polyacrylamide-Gel from Electron-Micrographs." Polymer ***25***(10): 1419-1423.

Hu, H. and R. G. Larson (2002). "Evaporation of a Sessile Droplet on a Substrate." The Journal of Physical Chemistry B **106**(6): 1334-1344.

Hu, H. and R. G. Larson (2005). "Analysis of the Effects of Marangoni Stresses on the Microflow in an Evaporating Sessile Droplet." Langmuir **21**(9): 3972-3980.

Hu, H. and R. G. Larson (2005). "Analysis of the Microfluid Flow in an Evaporating Sessile Droplet." Langmuir **21**(9): 3963-3971.

Jing, J., J. Reed, et al. (1998). "Automated high resolution optical mapping using arrayed, fluid-fixed DNA molecules." Proceedings of the National Academy of Sciences **95**(14): 8046-8051.

Kaganer, V. M., H. Möhwald, et al. (1999). "Structure and phase transitions in Langmuir monolayers." Reviews of Modern Physics **71**(3): 779-819.

Keng, P. Y., I. Shim, et al. (2007). "Synthesis and Self-Assembly of Polymer-Coated Ferromagnetic Nanoparticles." ACS Nano **1**(4): 279-292.

Khanal, B. P. and E. R. Zubarev (2007). "Rings of Nanorods." Angewandte Chemie **119**(13): 2245-2248.

Kim, H. S., C. H. Lee, et al. (2010). "Nanoparticle Stripes, Grids, and Ribbons Produced by Flow Coating." Advanced Materials **22**(41): 4600-4604.

Kim, M., S. M. Anthony, et al. (2009). "Activated Surface Diffusion in a Simple Colloid System." Physical Review Letters **102**(17): 178303.

Kizilay, M. Y. and O. Okay (2003). "Effect of hydrolysis on spatial inhomogeneity in poly(acrylamide) gels of various crosslink densities." Polymer ***44***(18): 5239-5250.

Kyung-Young, J., F. L. Teixeira, et al. (2007). "Au/SiO_2 Nanoring Plasmon Waveguides at Optical Communication Band." Lightwave Technology, Journal of **25**(9): 2757-2765.

Lee, D. Y., J. T. Pham, et al. (2013). "Macroscopic Nanoparticle Ribbons and Fabrics." Advanced Materials **25**(9): 1248-1253.

Lorke, A., R. Johannes Luyken, et al. (2000). "Spectroscopy of Nanoscopic Semiconductor Rings." Physical Review Letters **84**(10): 2223-2226.

Lu, N., X. Chen, et al. (2004). "Lateral Patterning of Luminescent CdSe Nanocrystals by Selective Dewetting from Self-Assembled Organic Templates." Nano Letters **4**(5): 885-888.

Lutolf, M. P. (2009). "Biomaterials: Spotlight on hydrogels." Nat Mater ***8***(6): 451-453.

Mallam, S., F. Horkay, et al. (1989). "Scattering and Swelling Properties of Inhomogeneous Polyacrylamide Gels." Macromolecules ***22***(8): 3356-3361.

Mason, T. G., K. Ganesan, et al. (1997). "Particle Tracking Microrheology of Complex Fluids." Physical Review Letters **79**(17): 3282.

McCain, K. S., D. C. Hanley, et al. (2003). "Single-Molecule Fluorescence Trajectories for Investigating Molecular Transport in Thin Silica Sol−Gel Films." Analytical Chemistry **75**(17): 4351-4359.

Mei, B. C., K. Susumu, et al. (2009). "Polyethylene glycol-based bidentate ligands to enhance quantum dot and gold nanoparticle stability in biological media." Nat. Protocols **4**(3): 412-423.

Monthus, C. and J. P. Bouchaud (1996). "Models of traps and glass phenomenology." Journal of Physics a-Mathematical and General **29**(14): 3847-3869.

Montroll, E. W. and G. H. Weiss (1965). "Random Walks on Lattices .2." Journal of Mathematical Physics **6**(2): 167.

Moore, B. G., C. M. Knobler, et al. (1990). "Phase diagram of Langmuir monolayers of pentadecanoic acid: quantitative comparison of surface pressure and fluorescence microscopy results." The Journal of Physical Chemistry **94**(11): 4588-4595.

Murcia, M. J., D. E. Minner, et al. (2008). "Design of Quantum Dot-Conjugated Lipids for Long-Term, High-Speed Tracking Experiments on Cell Surfaces." Journal of the American Chemical Society **130**(45): 15054-15062.

Pauzauskie, P. J., D. J. Sirbuly, et al. (2006). "Semiconductor Nanowire Ring Resonator Laser." Physical Review Letters **96**(14): 143903.

Pelham, R. J. and Y.-l. Wang (1997). "Cell locomotion and focal adhesions are regulated by substrate flexibility." Proceedings of the National Academy of Sciences ***94***(25): 13661-13665.

Petsi, A. J. and V. N. Burganos (2006). "Evaporation-induced flow in an inviscid liquid line at any contact angle." Physical Review E **73**(4): 041201.

Pham, J. T., J. Lawrence, et al. (2013). "Highly Stretchable Nanoparticle Helices Through Geometric Asymmetry and Surface Forces." Advanced Materials: 1-6.

Pons, T., H. T. Uyeda, et al. (2006). "Hydrodynamic Dimensions, Electrophoretic Mobility, and Stability of Hydrophilic Quantum Dots." The Journal of Physical Chemistry B ***110***(41): 20308-20316.

Ramakrishna, G., Q. Dai, et al. (2007). "Interparticle Electromagnetic Coupling in Assembled Gold-Necklace Nanoparticles." Journal of the American Chemical Society **129**(7): 1848-1849.

Richards, E. G. and C. J. Temple (1971). "Some Properties of Polyacrylamdie Gels." Nature Physical Science ***230***: 92-96.

Roeffaers, M. B. J., B. F. Sels, et al. (2006). "Spatially resolved observation of crystal-face-dependent catalysis by single turnover counting." Nature **439**(7076): 572-575.

Ruchel, R., R. Steere, et al. (1978). "Tansmission electron microscopic observation of freeze etched polyacrylamide gels." Journal of Chromatography ***166***: 563.

Saltzman, E. J. and K. S. Schweizer (2008). "Large-amplitude jumps and non-Gaussian dynamics in highly concentrated hard sphere fluids." Physical Review E **77**(5): 051504.

Savin, T. and P. S. Doyle (2007). "Statistical and sampling issues when using multiple particle tracking." Physical Review E **76**(2): 021501.

Saxton, M. J. (2008). "Single-particle tracking: connecting the dots." Nat Meth **5**(8): 671-672.

Saxton, M. J. and K. Jacobson (1997). "SINGLE-PARTICLE TRACKING:Applications to Membrane Dynamics." Annual Review of Biophysics and Biomolecular Structure **26**(1): 373-399.

Scalas, E. (2006). "The application of continuous-time random walks in finance and economics." Physica A: Statistical Mechanics and its Applications **362**(2): 225-239.

Scalfani, V. F. and T. S. Bailey (2011). "Access to Nanostructured Hydrogel Networks through Photocured Body-Centered Cubic Block Copolymer Melts." Macromolecules ***44***(16): 6557-6567.

Schmidt, T., G. J. Schutz, et al. (1996). "Imaging of single molecule diffusion." Proceedings of the National Academy of Sciences of the United States of America **93**(7): 2926-2929.

Schultz, K. M., A. D. Baldwin, et al. (2009). "Gelation of Covalently Cross-Linked PEG−Heparin Hydrogels." Macromolecules **42**(14): 5310-5316.

Senses, E., M. Black, et al. (2013). "Spatial Ordering of Colloids in a Drying Aqueous Polymer Droplet." Langmuir **29**(8): 2588-2594.

Shibayama, M. (1998). "Spatial inhomogeneity and dynamic fluctuations of polymer gels." Macromolecular Chemistry and Physics ***199***(1): 1-30.

Steven, F. L. and A. O. Mark (2009). "Brightening, Blinking, Bluing and Bleaching in the Life of a Quantum Dot: Friend or Foe?" ChemPhysChem **10**(13): 2174-2191.

Sudeep, P. K., K. T. Early, et al. (2008). "Monodisperse Oligo(phenylene vinylene) Ligands on CdSe Quantum Dots: Synthesis and Polarization Anisotropy Measurements." Journal of the American Chemical Society ***130***(8): 2384-2385.

Sumner, A. L., E. J. Menke, et al. (2004). "The nature of water on surfaces of laboratory systems and implications for heterogeneous chemistry in the troposphere." Physical Chemistry Chemical Physics **6**(3): 604-613.

Susumu, K., B. C. Mei, et al. (2009). "Multifunctional ligands based on dihydrolipoic acid and polyethylene glycol to promote biocompatibility of quantum dots." Nat. Protocols **4**(3): 424-436.

Tada, H., H. Higuchi, et al. (2007). "In vivo Real-time Tracking of Single Quantum Dots Conjugated with Monoclonal Anti-HER2 Antibody in Tumors of Mice." Cancer Research **67**(3): 1138-1144.

Tang, Z., N. A. Kotov, et al. (2002). "Spontaneous Organization of Single CdTe Nanoparticles into Luminescent Nanowires." Science **297**(5579): 237-240.

Truskett, V. N. and K. J. Stebe (2003). "Influence of Surfactants on an Evaporating Drop: Fluorescence Images and Particle Deposition Patterns." Langmuir **19**(20): 8271-8279.

Uyeda, H. T., I. L. Medintz, et al. (2005). "Synthesis of Compact Multidentate Ligands to Prepare Stable Hydrophilic Quantum Dot Fluorophores." Journal of the American Chemical Society **127**(11): 3870-3878.

Valentine, M. T., P. D. Kaplan, et al. (2001). "Investigating the microenvironments of inhomogeneous soft materials with multiple particle tracking." Physical Review E **64**(6): 061506.

Wang, B., S. M. Anthony, et al. (2009). "Anomalous yet Brownian." Proceedings of the National Academy of Sciences **106**(36): 15160-15164.

Weigel, A. V., B. Simon, et al. (2011). "Ergodic and nonergodic processes coexist in the plasma membrane as observed by single-molecule tracking." Proceedings of the National Academy of Sciences **108**(16): 6438-6443.

Weiss, N. and A. Silberberg (1977). "Inhomogeneity of polyacrylamide gel structure from permeability and viscoelasticity." British Polymer Journal ***9***(2): 144-150.

Werts, M. H. V., M. Lambert, et al. (2001). "Nanometer Scale Patterning of Langmuir−Blodgett Films of Gold Nanoparticles by Electron Beam Lithography." Nano Letters **2**(1): 43-47.

Wong, I. Y., M. L. Gardel, et al. (2004). "Anomalous Diffusion Probes Microstructure Dynamics of Entangled F-Actin Networks." Physical Review Letters **92**(17): 178101.

Xue, J. Z., D. J. Pine, et al. (1992). "Nonergodicity and light scattering from polymer gels." Physical Review A **46**(10): 6550-6563.

Yeung, T., P. C. Georges, et al. (2005). "Effects of substrate stiffness on cell morphology, cytoskeletal structure, and adhesion." Cell Motility and the Cytoskeleton ***60***(1): 24-34.

Yildiz, A., J. N. Forkey, et al. (2003). "Myosin V Walks Hand-Over-Hand: Single Fluorophore Imaging with 1.5-nm Localization." Science **300**(5628): 2061-2065.

Yu, W. W., L. Qu, et al. (2003). "Experimental Determination of the Extinction Coefficient of CdTe, CdSe, and CdS Nanocrystals." Chemistry of Materials ***15***(14): 2854-2860.

Yunker, P. J., T. Still, et al. (2011). "Suppression of the coffee-ring effect by shape-dependent capillary interactions." Nature **476**(7360): 308-311.

Zhang, J., C. R. Daubert, et al. (2005). "Characterization of polyacrylamide gels as an elastic model for food gels." Rheologica Acta ***44***(6): 622-630.

Zhu, J.-H., F. Shao, et al. (2006). "Acrylamide as cosurfactant and hydrotrope in the pseudoternary Span 80-Tween 85/isopar M/water emulsion/microemulsion forming system." Colloids and Surfaces A: Physicochemical and Engineering Aspects **290**(1–3): 19-24.